water

MDPI

Article

Flow at an Ogee Crest Axis for a Wide Range of Head Ratios: Theoretical Model

Frédéric Stilmant [1], Sebastien Erpicum [1], Yann Peltier [2], Pierre Archambeau [1], Benjamin Dewals [1] and Michel Pirotton [1,*]

[1] Hydraulics in Environmental and Civil Engineering (HECE), Research Unit Urban & Environmental Engineering (UEE), University of Liège, 4000 Liège, Belgium; frederic_stilmant@yahoo.fr (F.S.); s.erpicum@uliege.be (S.E.); pierre.archambeau@uliege.be (P.A.); b.dewals@uliege.be (B.D.)

[2] Artelia, BU Villes & Territoires, Agence des Hauts-de-France, 59520 Marquette-lez-Lille, France; yann.peltier@arteliagroup.com

* Correspondence: michel.pirotton@uliege.be

Abstract: The discharge coefficient of an ogee crest is a function of the ratio of the effective head to the design head. The purpose of the present study is to derive a theoretical model of this relation, which does not depend on empirical coefficients and whose predictions over a wide range of head ratios are accurate enough for practical use. The developments consider unsubmerged ogee crests without approach flow or lateral contraction effects, heads large enough to enable surface tensions to be neglected, and heads small enough to avoid flow separation. The method is based on potential flow theory, depth integration in a curvilinear reference frame, and critical flow theory. The characteristics of the crest shape are defined by the trajectory of a free jet passing over the crest at the design head. The dimensionless equations show that the position of the critical section is not at the apex of the crest. Nevertheless, they also suggest an approximate equation at the apex of the crest from which the discharge coefficient is derived, together with the local water depth, velocity, and pressure distribution. The results compare well with experimental data for head ratios between 0 and 5, which validates the underlying assumptions of the theoretical model.

Keywords: ogee spillway; discharge coefficient; curvilinear flow; critical section

Citation: Stilmant, F.; Erpicum, S.; Peltier, Y.; Archambeau, P.; Dewals, B.; Pirotton, M. Flow at an Ogee Crest Axis for a Wide Range of Head Ratios: Theoretical Model. *Water* **2022**, *14*, 2337. https://doi.org/10.3390/w14152337

Academic Editor: Wencheng Guo

Received: 18 June 2022
Accepted: 22 July 2022
Published: 28 July 2022

Publisher's Note: MDPI stays neutral with regard to jurisdictional claims in published maps and institutional affiliations.

1. Introduction

Two essential physical properties of ogee crests are their discharge coefficient and the pressure profile along their invert. The discharge coefficient, C_d, is a measure of the spillway's hydraulic efficiency and is defined here as:

$$C_d = \frac{q}{\sqrt{2gH^3}} \quad (1)$$

where q is the discharge rate per unit width (m²/s), H is the upstream head, and g is the gravitational acceleration [1]. On the other hand, the concern for crest pressures is a matter of safety, since a pressure below the atmospheric pressure can favor flow detachment or can cause cavitation damage if it decreases close to the vapor pressure of water [2]. Therefore, the design of ogee crests aims for a high discharge coefficient while avoiding too small pressures. This is achieved by designing the crest shape according to the trajectory of the lower nappe of a fully ventilated flow over a sharp-crested weir—the head, H_d, of this design flow being the design head of the spillway [1,3].

The discharge coefficient and crest pressures are connected in the sense that they both vary when the upstream head, H, varies. However, research has also shown that different crest shapes can lead to very different pressure distributions on the crest while

having almost the same discharge coefficient, which has led to improved designs and to a greater interest in high–head operation, i.e., operation under heads significantly larger than H_d [4–6]. As a result, a better understanding of the connections between the crest shape, the operating head, the discharge coefficient, and the crest pressures is a relevant task [7].

A first approach to understanding these connections is based on the comparison of the plane flow over an ogee crest with the plane flow over a sharp-crested weir, as shown in Figure 1 [1,8], with both structures having an infinite height. For $H = H_d$, both flows are almost the same, despite the difference in the lower boundary condition (atmospheric pressure versus crest invert); in particular, the discharge coefficient is the same, and the pressures on the ogee crest equal atmospheric pressure. For $H \neq H_d$, the Froude similarity states that the thickness of the jet flow is identical to that of the design flow scaled by H/H_d and that the discharge coefficient remains the same. In comparison to this jet flow, the flow over the ogee crest is required to have a lower boundary with a different curvature, i.e., the curvature of the fixed spillway crest (nappe separation is not considered here). This difference suggests that the discharge coefficient and crest pressures must be different from those of the design flow.

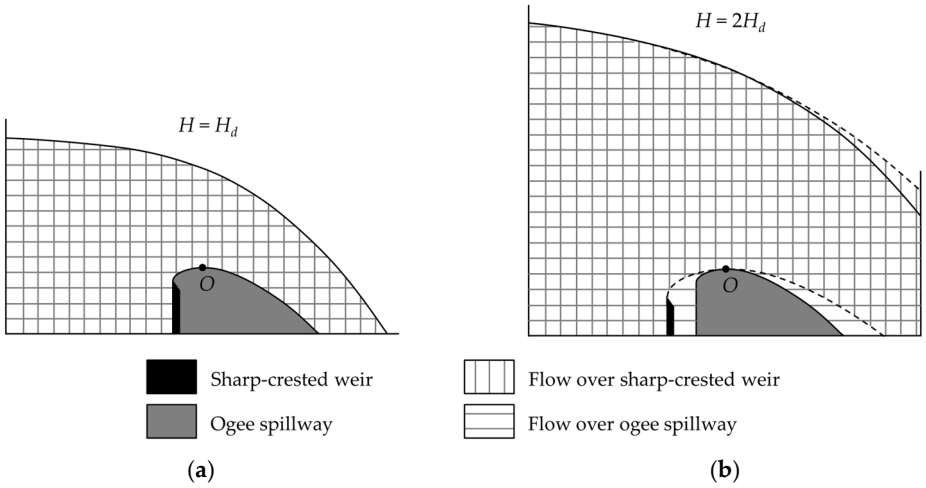

Figure 1. Comparison of flows over sharp-crested weir and ogee crest for two heads (heads are measured from point O): (**a**) design head; (**b**) effective head larger than the design head.

Three basic concepts are commonly used to explain the variation in discharge coefficient and pressures: potential (i.e., irrotational) flow theory, depth integration, and critical flow theory [7,9]. These need some introductory remarks.

The hydraulic behavior of ogee crests has been the subject of in-depth experimental studies with measurements of the discharge coefficient, crest pressures, free surface profile, flow velocities, and flow pressures [5,6,10–15]. Numerical models of ogee crests have been developed based on two-dimensional potential flow theory in a vertical plane and compared to experimental data [16–20]. The accuracy of their results (free surface profile, discharge coefficient, and crest pressure) underlined the validity of the approximation of potential flow—and therefore also the Bernoulli equation—for flows over ogee crests as long as they do not separate from the structure [16]. This is because these flows experience dramatic changes over a length that is short enough for the boundary layer to remain small [7]. Neglecting the boundary layer leads to slight overestimations of the discharge coefficient, i.e., <2% according to [12,16,21] and <0.3% according to [19]. Moreover, numerical simulations involving the three-dimensional Navier–Stokes equations with turbulence have been applied to flows on ogee crests [21–23]. They show that the free surface profile and crest pressures remain almost unaffected by surface roughness, while the discharge coefficient and the details of the velocity field are improved by introducing surface

roughness [21]. These simulations also make it clear that potential flow theory is no longer applicable in the case of flow separation, i.e., for very large head ratios [23].

Depth integration is a procedure that reduces the complexity of the system of equations and the number of variables (e.g., discharge instead of local velocities). In the case of plane flows, it reduces a two-dimensional set of equations to one dimension by discriminating between the direction of flow and the direction perpendicular to it, and it introduces the notion of cross sections. Depth integration depends on an assumption on the distribution of the flow velocities and pressures along the cross section (in the case of irrotational flows, the pressure distribution is linked to the velocity distribution, assuming constant head). This assumption is key to the performance and limitations of any one-dimensional model [7]. For curvilinear flows, depth integration is either performed in a fixed Cartesian coordinate system [7] or in a curvilinear reference system [7,24,25], and the basic assumption for the velocity and pressure distributions is an assumption of the distribution of the (radius of the) curvature of the streamlines intersecting a cross section. A strength of this approach is that, for flows on ogee crests without separation, the radius of the curvature at the flow–structure interface is known. As reported by Castro-Orgaz and Hager [7], Boussinesq suggested that the streamlines intersecting a cross section share the same center of curvature, i.e., the radii of the curvature are distributed linearly, and there is neither contraction nor expansion of the streamlines. Dressler's model is based on the same assumption [24,25]. Jaeger [9] suggested a more general linear distribution, which can be interpreted as a first-order approximation of the actual more complex distribution, as shown by two-dimensional simulations [7,26–28]. In the context of quasi-circular weirs, he found that the additional parameter of this distribution has only a weak influence on the discharge coefficient [9]. As reported by Castro-Orgaz and Hager [7], Fawer suggested a distribution of the curvatures (i.e., the inverse of the radii of curvature), but his distribution requires an approximate integration, with no significant improvement in the results.

Critical flow is a concept that arises from depth averaging the equations of motion. Even though the two-dimensional equations of potential flows are elliptic, which means that any point is influenced by the whole flow, the classical notion of critical flow states that, in the one-dimensional equations, there is one section that can be computed apart from the others and that determines the results in the other sections. Note, however, that this is not the case for all one-dimensional models that have been derived for curvilinear flows [7]. In some cases, critical flow is, rather, a concept imported from outside of the specific mathematical framework of a given model. Therefore, this topic needs a few remarks.

In the most basic form of the Bernoulli equation, the specific discharge, q, (assumed steady) at any section can be expressed as a function of the head, H, a measurement of the water depth, h, and other quantities such as the elevation of the channel bottom, which are known functions of the abscissa, ξ, of the section [29]:

$$q = f(H, h, \xi) \tag{2}$$

The conservation of mass and energy states that in this equation q and H are constant parameters. Therefore, from a mathematical point of view, Equation (2) is the implicit definition of a curve in the (ξ,h) plane. To fully describe this curve, the graphs of two functions of $h(\xi)$ are required. These are the subcritical $h_{sub}(\xi)$ and the supercritical $h_{sup}(\xi)$ branches of the curve defined by Equation (2) and shown in Figure 2, which are the only mathematical solutions that are physically acceptable, depending on the upstream and downstream boundary conditions of the flow.

The models that can be expressed in the form of Equation (2)—Jaeger's and Dressler's models [7,24,25] are two of them—have the property that their critical sections are singular points of the curve representing the evolution of the water depth, h, with abscissa ξ. In geometry, the curve defined by Equation (2) is said to have a singular point (ξ_c, h_c) if

$$\begin{cases} \left.\dfrac{\partial f}{\partial h}\right|_{(\xi_c, h_c)} = 0 \\ \left.\dfrac{\partial f}{\partial \xi}\right|_{(\xi_c, h_c)} = 0 \end{cases} \quad (3)$$

[30], i.e., if (ξ_c, h_c) is a critical point of function f [31]. Such a singular point can be a point where several branches of a curve intersect [30]. This is the case for curves defined by Equation (2): (ξ_c, h_c) is the intersection point of the subcritical and supercritical branches. This implies that any flow ranging from the large upstream to the small downstream water depths h needs to intersect this point (Figure 2), which, in the hydraulic sense, is the critical section of the flow. Its position, ξ_c, and value, h_c, are given by Equation (3) and are dependent on parameter H. Inserting ξ_c and h_c in Equation (2) gives the function q_c (H), which leads to the presence of a singular point on the curve, or, in other words, the head–discharge function of an overflow structure such as a spillway crest. Note that, according to Equation (3) and Figure 2, q_c is the largest discharge that can flow through the critical section, ξ_c.

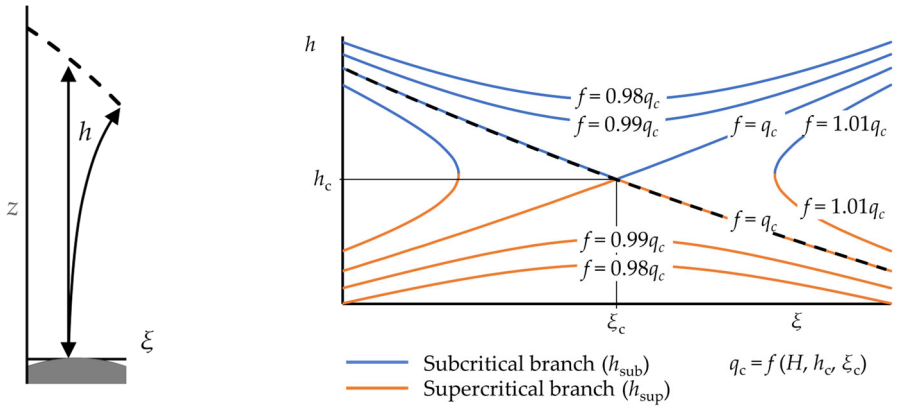

(**a**) (**b**)

Figure 2. (**a**) Possible definitions of abscissa ξ and water depth h; (**b**) Contour plot showing the values of function f (H, h, ξ) with their subcritical (in blue) and supercritical branches (in orange); the transcritical solution shown in (**a**) is also plotted in (**b**) (black dotted line); point (ξ_c, h_c) is a critical point of function f and a singular point of the corresponding subcritical and supercritical branches.

These developments are well-known from standard textbooks [29]. However, in some depth-averaged models—typically models based on the Boussinesq approach— the discharge, q, is not only a function of H, h, and ξ, as in Equation (2), but also of the derivatives of the water depth, $d^n h/d\xi^n$ (n = 1, 2, …) [7]. These spatial derivatives are included in order to increase the quality of the model by taking into account the flow velocities perpendicular to the main flow direction. However, at the same time, these derivatives lead to the loss of the property that the critical section is a singular point whose position and value are known apart from the rest of the curve. Only an iterative approach or the use of lower order approximations make it possible to continue to use critical flow theory with such models [7].

This discussion and the choice of the model are important here because these differences suggest that if the head–discharge function of a spillway crest is, as a first approximation, determined by a single cross section there are secondary effects through which the rest of the flow influences the behavior of the "critical" section. Experiments on ogee crests stress, on one hand, that the discharge coefficient mainly depends on a limited portion of the crest shape immediately upstream and downstream from the crest apex [5,13,14]; on the other hand, the discharge coefficient is also influenced by the approach depth and the upstream slope of the spillway [3,14,32]. As a result, a free-surface model

whose critical section is not influenced by the flow upstream and downstream is, at best, able to give a discharge coefficient for spillway crests not influenced by the approach conditions. In the case of a vertical upstream wall, this requires a spillway height at least three times that of the flow head [32,33].

Jaeger [9] developed a model for the discharge coefficient of quasi-circular weirs that uses the building blocks of irrotational flow, depth averaging, and critical flow. His model assumes that the critical section is at the highest point of the weir and that the discharge at that point is the maximum, i.e., the derivative of the discharge with respect to the water depth is zero. This theory gives the discharge coefficient as a function of the head, the critical water depth, and the radius of curvature of the weir [9]. Initially, compared to measurements on circular weirs [9,34], this model also compares well with data from ogee crests up to head ratios of $H/H_d = 3.7$ [7], which confirms the relevance of the building blocks he used. Castro-Orgaz [34] followed a similar approach but considered the constant parameter of Jaeger's model to be dependent on the water depth. This model gives good results for head ratios up to 2 [7,34]. Note, however, that ogee crests do not match Jaeger's hypothesis of a quasi-circular weir in a strict sense, which challenges his definition of the critical section.

These introductory remarks suggest that a theory based on irrotational flow, depth averaging, and critical flow is sufficient to model the behavior of ogee crests but that a more rigorous mathematical framework is necessary, especially when it comes to critical flow theory. This is the aim of the present study, which uses well-known approaches and assumptions and selects them in such a way as to allow for the highest accuracy while keeping an unambiguous definition of the critical section as a singular point and making a full analytical treatment of the equations whenever possible.

The outline of the developments is shown in Figure 3. Once the mathematical framework is set up (Sections 2.1 and 2.2), it is first applied to compute the jet flow whose lower boundary defines the profile of the spillway crest (Section 2.3). This solution gives the opportunity to assess the consistency of some assumptions (Section 2.4). The theoretical shape of an ogee crest (rather than any common definition of it) is then used as a boundary condition for the flow over the crest (Section 2.5). This choice avoids dealing with the discontinuities displayed by most of the ogee crest shapes used in practice [35], and it also has the advantage of providing a crest shape that is consistent with the theoretical frame of the free-surface flow model (i.e., the pressure on the structure is exactly atmospheric at the design head).

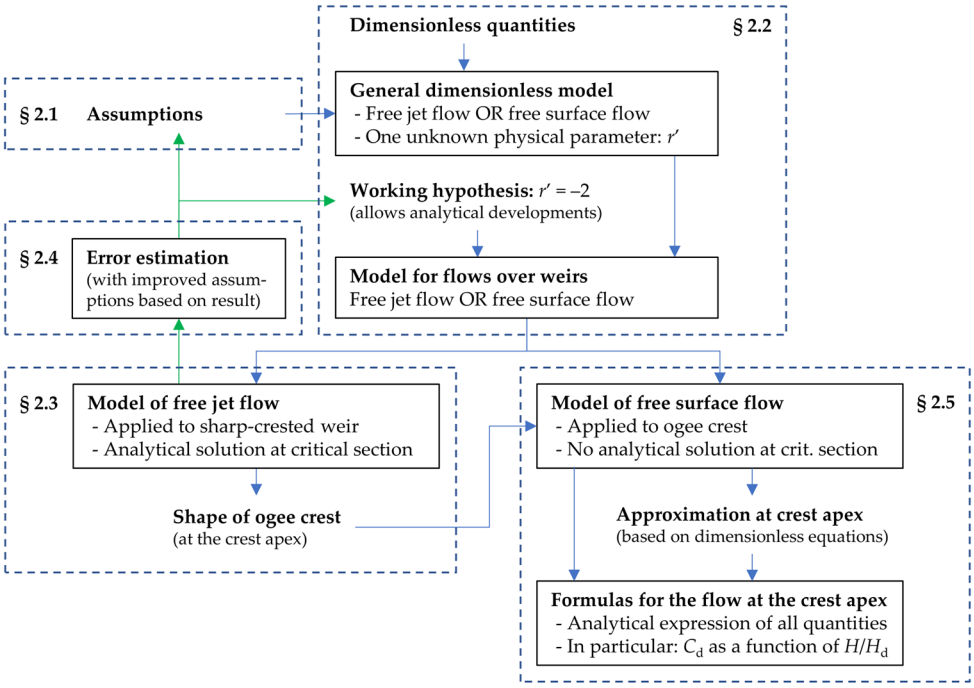

Figure 3. Outline of the development of the model, with reference to the Sections 2.1–2.5.

No empirical data are used in this procedure. Instead, all assumptions are guided by the wish to avoid any numerical treatment of the equations. The theoretical model is then compared to experimental data collected on physical models experiencing heads up to five times larger than the design head (Section 3). It is also compared to Jaeger's model in order to discuss the influence of the assumptions on the outputs of the model (Section 4).

The scope of the model is, however, restricted to unsubmerged ogee crests without any effect of approach flow velocity (reservoir application) or lateral contraction (piers or abutments). The model also does not consider surface tensions, making it only valid for heads larger than 5 cm [36], or the separation of the flow from the structure, which happens for heads several times larger than the design head.

2. Model Development

2.1. Assumptions

2.1.1. Curvilinear Coordinate System

The curvilinear coordinate system used in this paper was first introduced by Dressler [24]. Let Equation (4) be a parametric representation of the lower boundary of a two-dimensional flow in a vertical plane, where x and z are the horizontal and vertical coordinates of a Cartesian coordinate system and ξ is the natural parameter of the curve, and let the functions $x_b(\xi)$ and $z_b(\xi)$ be two-times differentiable.

$$\begin{cases} x = x_b(\xi) \\ z = z_b(\xi) \end{cases} \tag{4}$$

This curve, shown in Figure 4, is called the "reference curve". Let θ be its inclination with respect to the x-axis (with values between $-\pi/2$ and $\pi/2$) and r_b be its radius of curvature. These quantities are given by:

$$\theta(\xi) = \tan^{-1}\left(\frac{dz_b}{dx_b}\right) \tag{5}$$

$$r_b(\xi) = \left(\frac{d\theta}{d\xi}\right)^{-1} \tag{6}$$

Note that r_b is positive when the reference curve is locally convex and negative when it is locally concave.

Equation (5) is equivalent to:

$$\frac{\mathrm{d}x_b}{\mathrm{d}\xi} = \cos\theta \tag{7}$$

$$\frac{\mathrm{d}z_b}{\mathrm{d}\xi} = \sin\theta \tag{8}$$

Let η be the distance in the direction normal to the reference curve. With these definitions, Equation (9) is a change of variables between the Cartesian coordinate system (x, z) and an orthogonal curvilinear coordinate system (ξ, η).

$$\begin{cases} x = x_b(\xi) - \eta\sin[\theta(\xi)] \\ z = z_b(\xi) + \eta\cos[\theta(\xi)] \end{cases} \tag{9}$$

Transformation defined by Equation (9) is a one-to-one map as long as [24]:

$$\frac{\eta}{r_b} < 1 \tag{10}$$

When r_b is negative, Equation (10) is always true within the flow. Note that r_b can be measured along the η-axis (see Figure 4, where r_b is negative).

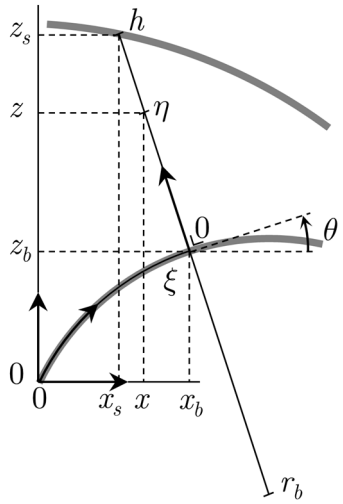

Figure 4. Definition of the curvilinear coordinate system and the quantities associated with it.

Let h be the distance between the lower and upper flow boundary measured along the local η-axis (Figure 4). The parametrization of the upper flow boundary is then:

$$\begin{cases} x_s(\xi) = x_b(\xi) - h\sin[\theta(\xi)] \\ z_s(\xi) = z_b(\xi) + h\cos[\theta(\xi)] \end{cases} \tag{11}$$

2.1.2. Conservation Principles

The absence of any gain or loss of mass or energy implies that the discharge and head are constant throughout the flow. This is valid in both the Cartesian and curvilinear coordinate systems.

Let q be the specific discharge at a cross section, ξ, defined as:

$$q(\xi) = \int_0^{h(\xi)} u(\xi, \eta)\,\mathrm{d}\eta \tag{12}$$

where u is the local velocity component normal to the cross section.

Let H be the head, defined as:

$$H(\xi) = z(\xi, \eta) + \frac{p(\xi, \eta)}{\rho g} + \frac{u^2(\xi, \eta) + w^2(\xi, \eta)}{2g} \tag{13}$$

where p is the local pressure, ρ is the density of water, and w is the local velocity component parallel to the cross section. Equation (13) assumes that all streamlines have the same head, which is consistent with the absence of any gain or loss of energy if all streamlines have the same head at the upstream boundary condition.

In the curvilinear coordinate system, the conservation principles read:

$$\frac{\mathrm{d}q}{\mathrm{d}\xi} = 0 \tag{14}$$

$$\frac{\mathrm{d}H}{\mathrm{d}\xi} = 0 \tag{15}$$

2.1.3. Velocity and Pressure Distributions

A one-dimensional approach requires assumptions on the velocity and pressure distributions along the η-axis, and the accuracy of the model depends on the quality of these assumptions. Actually, the velocity and pressure distributions are linked through Equation (13) so that only one distribution requires an assumption. Since function $u(\eta)$ needs to be integrated in Equation (12) and because u and w have a higher exponent than p in Equation (13), it is more convenient to make an assumption on the velocity distribution than on the pressure distribution. The conditions on the pressure, p, or elevation, z, at either the upper or lower flow boundary need to be considered in the assumed velocity distribution and therefore need to be converted into conditions on the local velocity by making use of Equation (13).

An irrotational velocity distribution is compatible with a flow without energy loss, and it can also take the boundary conditions at both the upper and lower flow boundaries into account (elevation, slope, curvature, and pressure). Dressler [24] derived such a velocity distribution in a curvilinear coordinate system, assuming that the velocities parallel to the cross section are negligible (see also [25]). This distribution considers the slope and curvature of the lower flow boundary. Dressler [24] assumed this lower boundary to be fixed, but the same velocity profile can also be used for jet flows.

In their study of the flow on an ogee crest, Peltier et al. [15] derived an irrotational velocity distribution along an isopotential line based on a first-order Taylor polynomial of the distribution of the radius of curvature of the streamlines crossing that isopotential line. This is shown in Figure 5a. This velocity distribution is more general than Dressler's because it considers the fact that both the slope and the curvature of the streamlines vary from the lower to the upper flow boundary. As a result, it can ensure the compatibility of the velocity profile with the slope and curvature, not only of the lower but also of the upper flow boundary.

Here, their equation is used to represent the velocity component perpendicular to the η-axis, while w is neglected (Figure 5b):

$$u(\eta) = u_\mathrm{b}\left(1 + r'\frac{h}{r_\mathrm{b}}\frac{\eta}{h}\right)^{\frac{1}{r'}}, \tag{16}$$

$$w(\eta) = 0, \tag{17}$$

where u_b is u at the lower flow boundary, r_b the radius of curvature of the lower flow boundary, and

$$r' = \left.\frac{\partial r}{\partial \eta}\right|_{\eta=0} \tag{18}$$

This is the partial derivative of the radius of curvature of the streamlines with respect to η. Note that this is also the approach followed by Jaeger [9]. Note also that $r' = -1$ corresponds to Dressler's distribution. Peltier et al. [15] used r' as a tuning parameter. A similar assumption is made here: r' will be assumed to be independent of the flow.

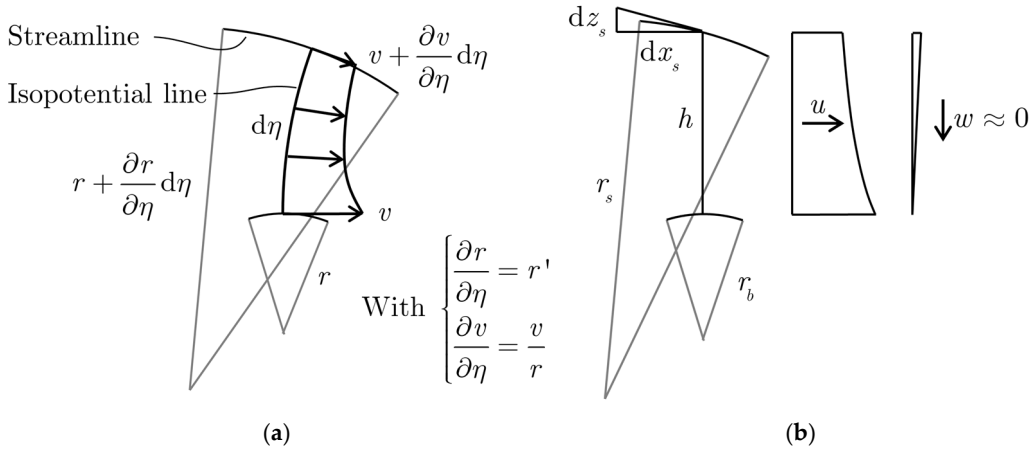

Figure 5. (**a**) Velocity distribution used by Peltier et al. [15], where v is the absolute velocity across an isopotential line, and r is the radius of curvature of the streamline; (**b**) Velocity distribution along the η-axis, where u is the velocity in direction ξ, and w is the velocity in direction η (neglected here).

2.1.4. Upper and Lower Boundary Conditions

All flows considered here have an upper boundary whose pressure is atmospheric. Setting this pressure as a reference, its value is 0, and the upper boundary condition reads:

$$p_s = p(h) = 0 \tag{19}$$

For the lower boundary condition, two types need to be distinguished [37]:

1. A lower boundary whose pressure is atmospheric, that is:

$$p_b = p(0) = 0 \tag{20}$$

2. A lower boundary whose shape is imposed by a fixed geometry, which means that the functions $x_b(\xi)$ and $z_b(\xi)$ in Equation (4) and all their derivatives are known prior to the computation of the flow.

2.2. Dimensionless Quantities and Equations

2.2.1. Velocity and Pressure Distribution Coefficients

Equation (16) makes it clear how the curvature of the streamlines influences the velocity distribution: as r_b/h tends toward infinity, the velocities tend to be constant across the flow (as in the shallow water equations), while as r_b/h tends to 0, the difference between the upper and lower velocities increases.

To simplify further developments, it is convenient to substitute r_b/h with another dimensionless variable that is directly measurable on the velocity profile defined in Equation (16). This quantity is λ, the ratio of the lower and upper velocities, u_b and u_s, which, according to Equation (16), is:

$$\lambda = \frac{u_b}{u_s} = \frac{u(0)}{u(h)} = \left(1 + r' \frac{h}{r_b}\right)^{-\frac{1}{r'}} \tag{21}$$

As shown in Figure 6, λ quantifies the uniformity of the dimensionless velocity profile. It is a velocity distribution coefficient but is different from the standard Coriolis or Boussinesq coefficients [29]. For parallel flows, λ equals 1.

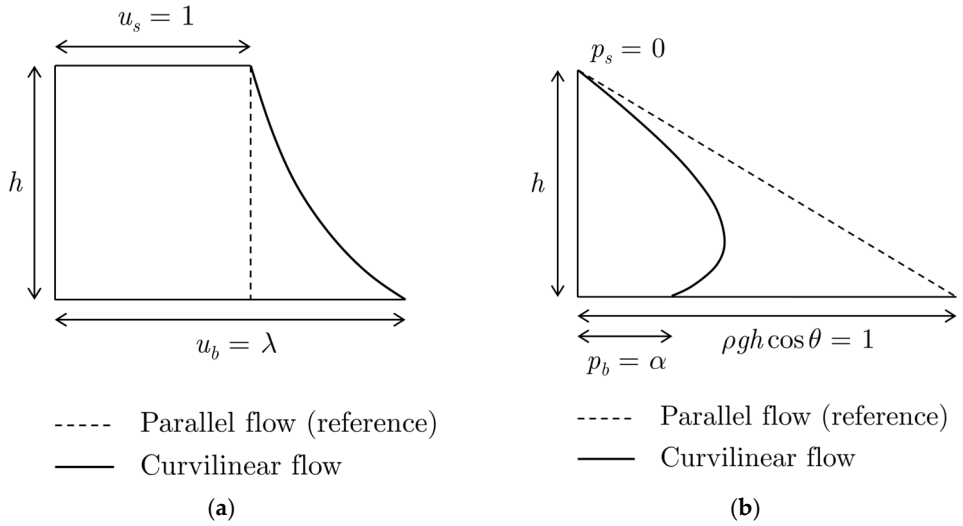

Figure 6. Definition of (**a**) velocity distribution coefficient λ and (**b**) pressure distribution coefficient α with reference to parallel flows.

In a similar way, it is also convenient to define a pressure distribution coefficient, α, as the ratio of the bottom pressure, p_b, to the hydrostatic value, $\rho g h \cos\theta$, that it would take if the flow had no curvature:

$$\alpha = \frac{p_b}{\rho g h \cos\theta} \tag{22}$$

As shown in Figure 6, α quantifies the linearity of the dimensionless pressure profile. It is, however, different from the standard pressure coefficients [29]. For parallel flows, α equals 1.

2.2.2. Equations with λ and α as Unknowns

Inverting Equation (21), the radius, r_b, becomes a function of λ:

$$r_b = h \frac{r'}{\lambda^{-r'} - 1} \tag{23}$$

With Equation (23), the velocity distribution Equation (16) becomes:

$$u(\eta) = u_b \left[1 - \left(1 - \lambda^{-r'} \right) \frac{\eta}{h} \right]^{\frac{1}{r'}} \tag{24}$$

Given Equations (11), (13), (17) and (24), the implication of the upper boundary condition defined in Equation (19) for the velocity distribution is:

$$u_b^2 = 2g\left(H - z_b - h\cos\theta \right) \lambda^2 \tag{25}$$

With Equations (13), (17) and (24), both lower boundary conditions can be expressed as Equation (26), where either p_b or z_b is known:

$$\frac{p_b}{\rho g} = H - z_b - \frac{u_b^2}{2g} \tag{26}$$

With Equations (22) and (25), the bottom boundary condition (Equation (26)) reads:

$$h = \frac{H - z_b}{\cos\theta} \frac{\lambda^2 - 1}{\lambda^2 - \alpha} \tag{27}$$

With Equation (27), Equation (23) reads:

$$r_b = \frac{H - z_b}{\cos\theta} r' \frac{\lambda^2 - 1}{\left(\lambda^{-r'} - 1\right)\left(\lambda^2 - \alpha\right)} \tag{28}$$

Integrating the velocity profile defined in Equation (24) on the cross section and taking the upper and lower boundary conditions defined in Equations (27) and (28) into account, the discharge rate defined in Equation (12) becomes:

$$q = \sqrt{2g} \frac{\left(H - z_b\right)^{3/2}}{\cos\theta} \frac{r'}{r'+1} \left[\frac{1-\alpha}{\left(\lambda^2 - \alpha\right)^3}\right]^{1/2} \frac{\left(\lambda^2 - 1\right)\left(\lambda^{-r'} - \lambda\right)}{\left(\lambda^{-r'} - 1\right)} \tag{29}$$

Note that for $r' = -1$, this expression is indefinite and needs to be replaced by its limit [24,25].

2.2.3. Design Head, H_d, as a Reference for all Other Dimensionless Variables

Equations (27) and (28) suggest defining a dimensionless depth, radius of curvature, and discharge rate with the help of the specific head (H–z_b). However, this quantity has two drawbacks. First, it is not constant over space (because of z_b), which changes the behavior of the derivatives of the corresponding dimensionless quantities with respect to the original ones (e.g., they do not become 0 simultaneously). Second, it is not the same for all flows over a given structure, while studying different flows over the same structure is the aim of this study. For these reasons, it is convenient to use a characteristic length of the fixed shape of the structure to define dimensionless quantities. In the case of ogee crests, this quantity is the design head, H_d:

$$\overline{\xi} = \frac{\xi}{H_d}, \quad \overline{H} = \frac{H}{H_d}, \quad \overline{h} = \frac{h}{H_d}, \quad \overline{x}_b = \frac{x_b}{H_d}, \quad \overline{z}_b = \frac{z_b}{H_d}, \quad \overline{r}_b = \frac{r_b}{H_d} \tag{30}$$

$$\overline{q} = \frac{q}{\sqrt{2gH_d^3}} \tag{31}$$

Note that Equation (31) is not a standard discharge coefficient. Rather, the discharge coefficient, C_d, is given by:

$$C_d = \frac{\overline{q}}{\overline{H}^{3/2}} \tag{32}$$

2.2.4. Set of Dimensionless Equations

With Equations (30) and (31), Equations (27) to (28) result in:

$$\overline{q} = \frac{\left(\overline{H} - \overline{z}_b\right)^{3/2}}{\cos\theta} \frac{r'}{r'+1} \left[\frac{1-\alpha}{\left(\lambda^2 - \alpha\right)^3}\right]^{1/2} \frac{\left(\lambda^2 - 1\right)\left(\lambda^{-r'} - \lambda\right)}{\left(\lambda^{-r'} - 1\right)} \tag{33}$$

$$\overline{h} = \frac{\overline{H} - \overline{z}_b}{\cos\theta} \frac{\lambda^2 - 1}{\lambda^2 - \alpha} \tag{34}$$

$$\overline{r}_b = \frac{\overline{H} - \overline{z}_b}{\cos\theta} r' \frac{\lambda^2 - 1}{\left(\lambda^{-r'} - 1\right)\left(\lambda^2 - \alpha\right)} \tag{35}$$

These three equations involve eight dimensionless quantities. Moreover, five independent first-order differential equations involving the same dimensionless variables plus two others are provided in Sections 2.1.1 (reference curve) and 2.1.2 (conservation principles). All these differential equations require an initial value.

With Equations (30) and (31), the dimensionless conservation principles (Equations (14) and (15)) are:

$$\frac{\mathrm{d}\overline{q}}{\mathrm{d}\overline{\xi}} = 0 \tag{36}$$

$$\frac{\mathrm{d}\overline{H}}{\mathrm{d}\overline{\xi}} = 0 \tag{37}$$

These equations simply state that $\overline{q}$ and $\overline{H}$ are constant and equal to their initial values.

The dimensionless equations of the reference curve (Equations (5), (6), (7) and (8)) are:

$$\theta(\xi) = \tan^{-1}\left(\frac{\mathrm{d}z_\mathrm{b}}{\mathrm{d}x_\mathrm{b}}\right) \tag{38}$$

$$\frac{\mathrm{d}\overline{x}_\mathrm{b}}{\mathrm{d}\overline{\xi}} = \cos\theta \tag{39}$$

$$\frac{\mathrm{d}\overline{z}_\mathrm{b}}{\mathrm{d}\overline{\xi}} = \sin\theta \tag{40}$$

$$\frac{\mathrm{d}\theta}{\mathrm{d}\overline{\xi}} = \frac{\cos\theta}{\overline{H} - \overline{z}_\mathrm{b}} \frac{1}{r'} \frac{\left(\lambda^2 - \alpha\right)\left(\lambda^{-r'} - 1\right)}{\left(\lambda^2 - 1\right)} \tag{41}$$

where Equation (41) makes use of Equation (35).

Depending on the lower boundary condition, some quantities are known before any computation of the flow, while others are unknown. This is shown in Table 1. In Table 1, both the dimensionless discharge and head are classified as known because they are the initial values of Equations (36) and (37). However, as stated by critical flow theory, unsubmerged flows on sharp-crested weirs and on ogee crests are such that an additional equation linking the two quantities appears. Deriving this critical-state equation for both flows is the aim of Sections 2.4 and 2.5.

Table 1. System of equations depending on the lower boundary condition.

Lower BC: Atmospheric Pressure			**Lower BC: Prescribed Shape**		
Known Values	**Unknown Values**	**Equations**	**Known Values**	**Unknown Values**	**Equations**
IV: $\begin{cases}\overline{q}\\ \overline{H}\\ \overline{x}_{\mathrm{b},0}\\ \overline{z}_{\mathrm{b},0}\\ \theta_0\end{cases}$	$\begin{cases}\lambda(\overline{\xi})\\ \overline{z}_\mathrm{b}(\overline{\xi})\\ \theta(\overline{\xi})\end{cases}$	$\begin{cases}(33)\\ (40)\\ (41)\end{cases}$	IV: $\begin{cases}\overline{q}\\ \overline{H}\end{cases}$		
	$\overline{x}_\mathrm{b}(\overline{\xi})$	(39)	BC: $\begin{cases}\overline{x}_\mathrm{b}(\overline{\xi})\\ \overline{z}_\mathrm{b}(\overline{\xi})\\ \theta(\overline{\xi})\\ \overline{r}_\mathrm{b}(\overline{\xi})\end{cases}$	$\begin{cases}\lambda(\overline{\xi})\\ \alpha(\overline{\xi})\end{cases}$	$\begin{cases}(33)\\ (35)\end{cases}$
BC: $\alpha = 0$	$\overline{h}(\overline{\xi})$	(34)		$\overline{h}(\overline{\xi})$	(34)
Other: r'			Other: r'		

Note: BC = boundary condition; IV = initial value.

2.2.5. Working Hypothesis on r'

To further study the set of equations defined above, a value needs to be set for parameter r'. The values that make further analytical developments possible are very scarce. The value

$$r' = -2 \tag{42}$$

is one of them and is used here. Hypothesis (42) is therefore not a classic "tuning parameter" that is chosen freely to minimize the error in the output of a model. Instead, it is

chosen to make further analytical developments possible, and it is shown that, for the flows studied here, this choice is not inconsistent with the outputs of the model and that it is in good agreement with various kinds of experimental data.

With this assumption, Equation (33) becomes:

$$\overline{q} = 2\frac{\left(\overline{H}-\overline{z}_{\mathrm{b}}\right)^{3/2}}{\cos\theta}\left[\frac{1-\alpha}{\left(\lambda^2-\alpha\right)^3}\right]^{1/2}\left(\lambda^2-\lambda\right) \tag{43}$$

Equations (35) and (41) become:

$$\overline{r}_{\mathrm{b}} = -2\frac{\overline{H}-\overline{z}_{\mathrm{b}}}{\cos\theta}\frac{1}{\lambda^2-\alpha} \tag{44}$$

$$\frac{\mathrm{d}\theta}{\mathrm{d}\overline{\xi}} = -\frac{\cos\theta}{\overline{H}-\overline{z}_{\mathrm{b}}}\frac{\lambda^2-\alpha}{2} \tag{45}$$

Note that from Equations (34) and (43):

$$\begin{aligned}\lambda &> 1\\ \alpha &< 1\end{aligned} \tag{46}$$

i.e., the model with $r' = -2$ is valid for convex flows ($\overline{r}_{\mathrm{b}} < 0$) only.

Moreover, Equations (34) and (43) give:

$$\frac{\overline{h}}{\overline{r}_{\mathrm{b}}} = -\frac{\lambda^2-1}{2} \tag{47}$$

2.3. Flow over a Sharp-Crested Weir

As shown in Table 1, a system of three equations needs to be solved to compute a fully ventilated jet flow (the two other equations can be solved afterwards). The first of these equations, i.e., Equation (43), displays the same basic behavior as Equation (2) from the Introduction, except that the functions $\overline{z}_{\mathrm{b}}\left(\overline{\xi}\right)$ and $\theta\left(\overline{\xi}\right)$ are not explicit. In Equation (43), λ plays the same role as h in Equation (2). Moreover, as shown in Figure 7, the flow over a sharp-crested weir is the transition from a flow with a ratio of $\overline{h}/\overline{r}_{\mathrm{b}}$ tending toward infinity (large $\overline{h}$ and small $\overline{r}_{\mathrm{b}}$) to a flow with a ratio of $\overline{h}/\overline{r}_{\mathrm{b}}$ tending toward 0 (small $\overline{h}$ and large $\overline{r}_{\mathrm{b}}$). According to Equation (47), this implies that λ decreases from infinity to 1. Therefore, the analogy between Equations (2) and (43) suggests that the curve describing the solution of Equation (43) in the $\left(\overline{\xi},\lambda\right)$ plane needs to intersect a singular point in a similar way as in Figure 2.

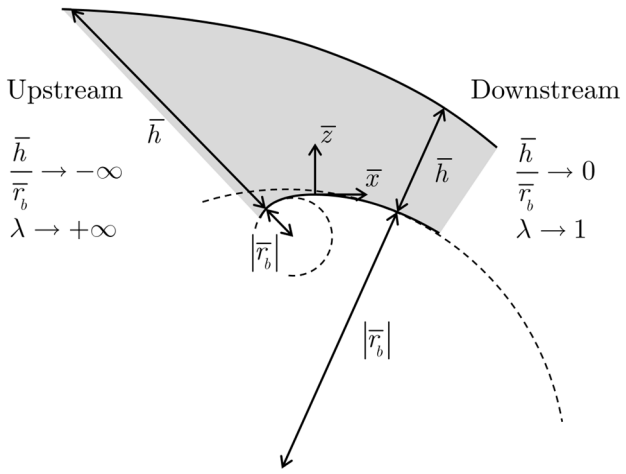

Figure 7. Evolution of λ along a flow over a sharp-crested weir.

As in Equation (3), this critical section is found by deriving Equation (43). This needs to take into account that free jet flows are characterized by $\alpha = 0$ and $\mathrm{d}\alpha / \mathrm{d}\overline{\xi} = 0$. Moreover, by the definition of the design head, H_d, the head ratio to consider here is $\overline{H} = 1$. With these assumptions, the derivation of Equation (43) gives:

$$-\frac{\lambda - 2}{\lambda(\lambda - 1)}\frac{\mathrm{d}\lambda}{\mathrm{d}\overline{\xi}} = -\left(1 - \frac{3}{2}\frac{\overline{r}_\mathrm{b}\cos\theta}{1 - \overline{z}_\mathrm{b}}\right)\frac{\tan\theta}{\overline{r}_\mathrm{b}} \tag{48}$$

The right-hand side is 0 when the lower nappe reaches its highest point (i.e., $\theta = 0$). With the exclusion of the limit state $\overline{r}_\mathrm{b} \to -\infty$, this is the only section at which it is 0. The left-hand side is a product of two factors, of which the second one is always negative since λ varies from infinity to 1 (Figure 7). With the exclusion of the limit state $\lambda \to +\infty$, the first factor is 0 if and only if $\lambda = 2$. As a result, the first factor of the left-hand side and the right-hand side need to be 0 simultaneously for Equation (48) to be verified, i.e., $\lambda = 2$ where $\theta = 0$. Since the equations are not dependent on the origin of $\overline{z}_\mathrm{b}$, let it be placed at this section:

$$\begin{cases} \overline{x}_{\mathrm{b},0} = \overline{x}_\mathrm{b}(0) = 0 \\ \overline{z}_{\mathrm{b},0} = \overline{z}_\mathrm{b}(0) = 0 \end{cases} \tag{49}$$

$$\theta_0 = \theta(0) = 0 \tag{50}$$

$$\lambda_0 = \lambda(0) = 2 \tag{51}$$

Then, according to Table 1 (with Equation (33) replaced with its differential form, Equation (48)), all flow features are known at the highest point of the lower boundary of the flow, and the features in the neighboring sections can be computed step by step with these values as initial values. As a result, there is a single solution in this dimensionless formulation of the problem that can transit from values of λ larger than 2 to values of λ smaller than 2.Despite the unusual variables, the section where $\lambda = 2$ and $\theta = 0$ is a critical section in the classical sense. One can verify that it corresponds to a maximum of $\overline{q}\cos\theta / (1 - \overline{z}_\mathrm{b})^{3/2}$ (i.e., a maximum value of discharge or a minimum value of specific head) when λ varies.

The flow features that can be computed at the critical section include the discharge from Equation (43) (which is therefore no longer independent from H), the water depth from Equation (34), and the radius of curvature from Equation (44):

$$\overline{q} = \frac{1}{2} \tag{52}$$

$$\overline{h}_0 = \overline{h}(0) = \frac{3}{4} \tag{53}$$

$$\overline{r}_{\mathrm{b},0} = \overline{r}_\mathrm{b}(0) = -\frac{1}{2} \tag{54}$$

Moreover, deriving Equation (48) at the critical section gives (note that the factors multiplying $\mathrm{d}^2\lambda / \mathrm{d}\overline{\xi}^2$ and $\mathrm{d}\overline{r}_\mathrm{b} / \mathrm{d}\overline{\xi}$ are both equal to 0 at the critical section):

$$\left.\frac{\mathrm{d}\lambda}{\mathrm{d}\overline{\xi}}\right|_0 = -\sqrt{14} \tag{55}$$

Then, deriving Equation (34) gives:

$$\left.\frac{\mathrm{d}\overline{h}}{\mathrm{d}\overline{\xi}}\right|_0 = -\frac{\sqrt{14}}{4} \tag{56}$$

while deriving Equation (44) gives:

$$\left.\frac{\mathrm{d}\overline{r}_\mathrm{b}}{\mathrm{d}\overline{\xi}}\right|_0 = -\frac{\sqrt{14}}{2} \tag{57}$$

Following the same procedure with the second derivative of Equations (48), (34), and (44) gives:

$$\left.\frac{\mathrm{d}^2\lambda}{\mathrm{d}\overline{\xi}^2}\right|_0 = 24 \tag{58}$$

$$\left.\frac{\mathrm{d}^2\overline{h}}{\mathrm{d}\overline{\xi}^2}\right|_0 = \frac{21}{4} \tag{59}$$

$$\left.\frac{\mathrm{d}^2\overline{r}_\mathrm{b}}{\mathrm{d}\overline{\xi}^2}\right|_0 = -\frac{3}{2} \tag{60}$$

In short, all quantities and all of their derivatives are known at the critical section.

2.4. Assessment of the Consistency of the Model

The analytical solutions at the critical section of a free jet flow make it possible to assess the consistency of the assumptions on the velocity distribution ($w = 0$ and $r' = -2$) and their impact on the value of the discharge. The approach followed here is to use the solution of the equations to derive a better estimate of the velocity distribution and to compute the corresponding discharge coefficient as in a fixed-point (Picard) iteration [7]. The difference between the initial discharge coefficient and the one given by this first iteration gives an order of magnitude of the error on C_d due to the approximations on the velocity distribution.

2.4.1. Slope of the Upper Flow Boundary and Assumption $w = 0$

The velocity distribution derived by Peltier et al. [15] applies to the absolute velocity, while in Equation (16) it has been applied to the velocity component perpendicular to the η-axis. To discuss the implications of this choice, let $u_\mathrm{est.}$ and $w_\mathrm{est.}$ be the velocity components in directions ξ and η if the velocity distribution derived by Peltier et al. [15] is applied to the absolute velocity. This would imply (after dividing by $\sqrt{2gH_\mathrm{d}}$):

$$\overline{u}_\mathrm{est.}^2 + \overline{w}_\mathrm{est.}^2 = \overline{u}^2 \tag{61}$$

Moreover, the velocity components $u_\mathrm{est.}$ and $w_\mathrm{est.}$ would be connected through the slopes of the streamlines crossing the η-axis. Assuming a linear variation in the inclination of the streamlines from the bottom "b" to the top "s", as suggested by the numerical results by Castro-Orgaz [28], would give:

$$\overline{w}_\mathrm{est.} = \tan\left(\left(\theta_\mathrm{s} - \theta\right)\frac{\overline{\eta}}{\overline{h}}\right)\overline{u}_\mathrm{est.} \tag{62}$$

where:

$$\theta_\mathrm{s} = \tan^{-1}\left(\frac{\mathrm{d}\overline{z}_\mathrm{s}}{\mathrm{d}\overline{x}_\mathrm{s}}\right). \tag{63}$$

The solutions for Equations (61) and (62) are:

$$\frac{\overline{u}_\mathrm{est.}}{\overline{u}} = \left[1 + \tan^2\left(\left(\theta_\mathrm{s} - \theta\right)\frac{\overline{\eta}}{\overline{h}}\right)\right]^{-1/2} \tag{64}$$

$$\frac{\overline{w}_\mathrm{est.}}{\overline{u}} = \tan\left(\left(\theta_\mathrm{s} - \theta\right)\frac{\overline{\eta}}{\overline{h}}\right)\left[1 + \tan^2\left(\left(\theta_\mathrm{s} - \theta\right)\frac{\overline{\eta}}{\overline{h}}\right)\right]^{-1/2} \tag{65}$$

These equations show that neglecting w is a valid approximation as long as:

$$\tan^2\left(\theta_s-\theta\right)<<1 \tag{66}$$

They also show that neglecting w implies lowering the level of connection between the flow features in a given section and the flow features in the neighboring sections.

The slope of the upper flow boundary is, with Equations (11), (34), (39), (40), and (45):

$$\tan\theta_s=\frac{\mathrm{d}\overline{z}_s}{\mathrm{d}\overline{x}_s}=\frac{\frac{\mathrm{d}\overline{z}_s}{\mathrm{d}\overline{\xi}}}{\frac{\mathrm{d}\overline{x}_s}{\mathrm{d}\overline{\xi}}}=\frac{\frac{\mathrm{d}\overline{h}}{\mathrm{d}\overline{\xi}}\cos\theta+\frac{1+\lambda^2}{2}\sin\theta}{-\frac{\mathrm{d}\overline{h}}{\mathrm{d}\overline{\xi}}\sin\theta+\frac{1+\lambda^2}{2}\cos\theta} \tag{67}$$

With the values from Section 2.4, the slope at the crest apex is:

$$\tan\theta_{s,0}=\left.\frac{\mathrm{d}\overline{z}_s}{\mathrm{d}\overline{x}_s}\right|_0=-\frac{\sqrt{14}}{10}\approx-0.374 \tag{68}$$

According to Equation (64), at the upper flow boundary, the neglected vertical velocity is 35% of the local velocity given by the model, while Equation (65) states that the horizontal velocity should be 94% of the value predicted by the model. This indicates, on one hand, that the vertical velocities in the critical section are not negligible at the design head, but on the other hand, their effect on the horizontal velocities is limited. Let us assess the impact of this simplification on the discharge coefficient.

With Equations (12), (16), (42), and (54), the discharge of the model can be written as:

$$\overline{q}=\overline{u}_{b,0}\int_0^{\overline{h}_0}\frac{\mathrm{d}\overline{\eta}}{\left(1+4\overline{\eta}\right)^{1/2}}=\frac{\overline{u}_{b,0}}{2}\left[\left(1+4\overline{h}_0\right)^{1/2}-1\right] \tag{69}$$

while the discharge corresponding to the better estimates of the velocities is:

$$\overline{q}_{est.}=\overline{u}_{b,0}\int_0^{\overline{h}_0}\frac{\frac{\overline{u}_{est.}}{\overline{u}}}{\left(1+4\overline{\eta}\right)^{1/2}}\mathrm{d}\overline{\eta} \tag{70}$$

With Equation (64), there is no analytical expression of the integral in Equation (70). Equation (64) is therefore replaced by its second-order Taylor polynomial:

$$\frac{u_{est.}}{u}\approx1-\frac{1}{2}\left(\theta_{s,0}\frac{\eta}{h_0}\right)^2 \tag{71}$$

Note that this approximation leads to a slight (<0.1%) overestimation of $\overline{u}_{s,est.}$. With Equation (70), Equation (71) becomes:

$$\overline{q}_{est.}=\frac{\overline{u}_{b,0}}{2}\left[\left(1+4\overline{h}_0\right)^{1/2}-1-\frac{5\left(1+4\overline{h}_0\right)^{1/2}-1}{60}\theta_{s,0}^2\right] \tag{72}$$

From Equation (69) and Equation (72):

$$\frac{C_d}{C_{d,est.}}=\frac{\overline{q}}{\overline{q}_{est.}}\approx1.02 \tag{73}$$

The estimated effect on the discharge coefficient of neglecting the effect of the vertical velocity component is, then, an overestimation by 2%. Note that, as stated in the Introduction, 2% is the precision that can be reached within the frame of potential flow theory.

2.4.2. Curvature of the Upper Flow Boundary and Assumption $r' = -2$

Another simplification has been made on the velocity profile, i.e., the dimensionless quantity r' has been assumed to be independent of the abscissa and the head. To discuss the implications of this choice, let $r'_{est.}$ be the derivative of the radius of curvature of the streamlines crossing the η-axis that would give a distribution compatible with the radius of curvature of the upper flow boundary:

$$r'_{\text{est.}} = \frac{\overline{r}_\text{s} - \overline{r}_\text{b}}{\overline{h}} \tag{74}$$

where, by definition of the radius of curvature:

$$\overline{r}_\text{s} = \frac{\left[1 + \left(\frac{\mathrm{d}\overline{z}_\text{s}}{\mathrm{d}\overline{x}_\text{s}}\right)^2\right]^{\frac{3}{2}}}{\frac{\mathrm{d}^2\overline{z}_\text{s}}{\mathrm{d}\overline{x}_\text{s}^2}} \tag{75}$$

Equation (74) suggests that assuming r' is independent of h is compatible with the underlying assumption that the radius of curvature varies linearly with η. This, however, does not guarantee by itself that assuming r' is independent of ξ is a valid hypothesis. Equation (74) also shows that neglecting this variation implies lowering the level of connection between the flow features in a given section and the flow features in the neighboring sections.

The second derivative of the upper flow boundary is, according to Equation (11):

$$\frac{\mathrm{d}^2\overline{z}_\text{s}}{\mathrm{d}\overline{x}_\text{s}^2} = \frac{\frac{\mathrm{d}}{\mathrm{d}\overline{\xi}}\left(\frac{\mathrm{d}\overline{z}_\text{s}}{\mathrm{d}\overline{x}_\text{s}}\right)}{\frac{\mathrm{d}\overline{x}_\text{s}}{\mathrm{d}\overline{\xi}}} \tag{76}$$

With the values from Section 2.4, the value at the crest apex is:

$$\left.\frac{\mathrm{d}^2\overline{z}_\text{s}}{\mathrm{d}\overline{x}_\text{s}^2}\right|_0 = -\frac{13}{25} \tag{77}$$

Therefore, the radius of curvature (75) of the upper flow boundary at the crest apex is:

$$\overline{r}_{\text{s},0} = -\frac{25}{13}\left(\frac{57}{50}\right)^{\frac{3}{2}} \approx -2.34 \tag{78}$$

With this value, the estimate of parameter r' as defined in Equation (74) is:

$$r'_{\text{est.}} \approx -2.45 \tag{79}$$

The error on r' is, thus, about 23%. This difference is not negligible, and the model is inconsistent in this regard. However, the question is how much this impacts on the discharge coefficient. Based on Equation (33), the ratio of C_d to its better estimate is:

$$\frac{C_\text{d}}{C_{\text{d,est.}}} = 2\frac{r'_{\text{est.}}+1}{r'_{\text{est.}}}\frac{1}{\lambda_0+1}\frac{\lambda_0^{-r'_{\text{est.}}}-1}{\lambda_0^{-r'_{\text{est.}}-1}-1} \approx 1.02 \tag{80}$$

The estimated error on the discharge coefficient is, again, an overestimation of about 2%. The fact that the estimated error due to the choice of $r' = -2$ is of the same order as the error due to neglecting the vertical velocity component ($w = 0$) suggests that the precision of the variation in the radius of curvature of the streamline is good enough with regards to the other approximations. Note, however, that both simplifications may be additive.

To conclude, assuming $w = 0$ and $r' = -2$ have been proven to be acceptable assumptions, not because they are accurate in themselves but because their effect on the discharge is small.

2.5. Flow over an Ogee Crest

2.5.1. System of Equations

In the case of an ogee crest, the shape of the lower flow boundary (i.e., $\overline{x}_\text{b}\left(\overline{\xi}\right), \overline{z}_\text{b}\left(\overline{\xi}\right)$, and all their derivatives) is known beforehand, while α is not but depends on the flow. As shown in Table 1, λ and α are the solutions of a system of two equations. The notion

of critical section appears in a similar way to what was conducted in Section 2.4, but it requires the derivative form of both Equations (43) and (44) (i.e., of Equations (33) and (35) with $r' = -2$).

The system of the derivatives of Equations (43) and (44) reads:

$$\begin{cases} A_\lambda \dfrac{\mathrm{d}\lambda}{\mathrm{d}\overline{\xi}} + A_\alpha \dfrac{\mathrm{d}\alpha}{\mathrm{d}\overline{\xi}} = S \\ B_\lambda \dfrac{\mathrm{d}\lambda}{\mathrm{d}\overline{\xi}} + B_\alpha \dfrac{\mathrm{d}\alpha}{\mathrm{d}\overline{\xi}} = T \end{cases}, \tag{81}$$

where:

$$A_\lambda = \frac{1}{\overline{q}} \frac{\partial \overline{q}}{\partial \lambda} = \frac{-\lambda^3 + 2\lambda^2 - 2\lambda\alpha + \alpha}{\lambda(\lambda - 1)(\lambda^2 - \alpha)} \tag{82}$$

$$A_\alpha = \frac{1}{\overline{q}} \frac{\partial \overline{q}}{\partial \alpha} = -\frac{\lambda^2 + 2\alpha - 3}{2(1 - \alpha)(\lambda^2 - \alpha)} \tag{83}$$

$$S = -\frac{1}{\overline{q}} \left(\frac{\partial \overline{q}}{\partial \theta} \frac{\mathrm{d}\theta}{\mathrm{d}\overline{\xi}} + \frac{\partial \overline{q}}{\partial \overline{z}_\mathrm{b}} \frac{\mathrm{d}\overline{z}_\mathrm{b}}{\mathrm{d}\overline{\xi}} \right) = -\left(1 - \frac{3}{2} \frac{\overline{r}_\mathrm{b} \cos\theta}{\overline{H} - \overline{z}_\mathrm{b}} \right) \frac{\tan\theta}{\overline{r}_\mathrm{b}} \tag{84}$$

$$B_\lambda = 2 \frac{\overline{H} - \overline{z}_\mathrm{b}}{\overline{r}_\mathrm{b} \cos\theta} \frac{1}{\overline{r}_\mathrm{b}} \frac{\partial \overline{r}_\mathrm{b}}{\partial \lambda} = 2\lambda \tag{85}$$

$$B_\alpha = 2 \frac{\overline{H} - \overline{z}_\mathrm{b}}{\overline{r}_\mathrm{b} \cos\theta} \frac{1}{\overline{r}_\mathrm{b}} \frac{\partial \overline{r}_\mathrm{b}}{\partial \alpha} = -1 \tag{86}$$

$$T = 2 \frac{\overline{H} - \overline{z}_\mathrm{b}}{\overline{r}_\mathrm{b} \cos\theta} \frac{1}{\overline{r}_\mathrm{b}} \left(\frac{\mathrm{d}\overline{r}_\mathrm{b}}{\mathrm{d}\xi} - \frac{\partial \overline{r}_\mathrm{b}}{\partial \overline{z}_\mathrm{b}} \frac{\mathrm{d}\overline{z}_\mathrm{b}}{\mathrm{d}\xi} - \frac{\partial \overline{r}_\mathrm{b}}{\partial \theta} \frac{\mathrm{d}\theta}{\mathrm{d}\xi} \right) = \frac{2}{\overline{r}_\mathrm{b}} \left[\frac{\overline{H} - \overline{z}_\mathrm{b}}{\overline{r}_\mathrm{b} \cos\theta} \frac{\mathrm{d}\overline{r}_\mathrm{b}}{\mathrm{d}\xi} + \left(1 - \frac{\overline{H} - \overline{z}_\mathrm{b}}{\overline{r}_\mathrm{b} \cos\theta} \right) \tan\theta \right] \tag{87}$$

Note that, because of Equation (46), the denominators in Equations (82) and (83) are different from zero. Moreover, A_α, B_λ, and B_α are never equal to zero. This is also the case for T: except for $\overline{H} = 0$, it is never equal to zero on an ogee crest, as suggested by Equations (54), (57) and (60)

Linear combinations of both equations in system 81 give:

$$\begin{cases} \left(1 - \dfrac{A_\lambda B_\alpha}{A_\alpha B_\lambda} \right) \dfrac{\mathrm{d}\lambda}{\mathrm{d}\overline{\xi}} = \dfrac{T}{B_\lambda} \left(1 - \dfrac{B_\alpha S}{A_\alpha T} \right) \\ \left(1 - \dfrac{A_\lambda B_\alpha}{A_\alpha B_\lambda} \right) \dfrac{\mathrm{d}\alpha}{\mathrm{d}\overline{\xi}} = \dfrac{T}{B_\alpha} \left(\dfrac{B_\alpha S}{A_\alpha T} - \dfrac{A_\lambda B_\alpha}{A_\alpha B_\lambda} \right) \end{cases} \tag{88}$$

Both equations in system (88) have the same shape as Equation (48), which suggests that the notion of a critical section also applies here. Because T is never equal to 0, the critical section is characterized by the following equations, where subscript "c" refers to the critical section:

$$\frac{A_{\lambda,\mathrm{c}} B_{\alpha,\mathrm{c}}}{A_{\alpha,\mathrm{c}} B_{\lambda,\mathrm{c}}} = 1 \tag{89}$$

$$\frac{B_{\alpha,\mathrm{c}} S_\mathrm{c}}{A_{\alpha,\mathrm{c}} T_\mathrm{c}} = 1 \tag{90}$$

Equation (84) shows that $S = 0$ at the highest point of the crest. Therefore, this point cannot verify Equation (90) and cannot be the critical section, even for the design head. This is due to the fact that, unlike circular weirs, $\mathrm{d}\overline{r}_\mathrm{b} / \mathrm{d}\overline{\xi}$ (and therefore T) is not equal to 0 at the apex of the crest. The details of the numerical computation of the position of the critical section are not presented here, but they show that, except for $\overline{H} = 0$, the critical section is slightly downstream of the crest apex, and its position depends on the head

ratio. As shown in Figure 8, the flow for the design head is identical to the design flow over the sharp-crested weir, except that it does not have the same critical section.

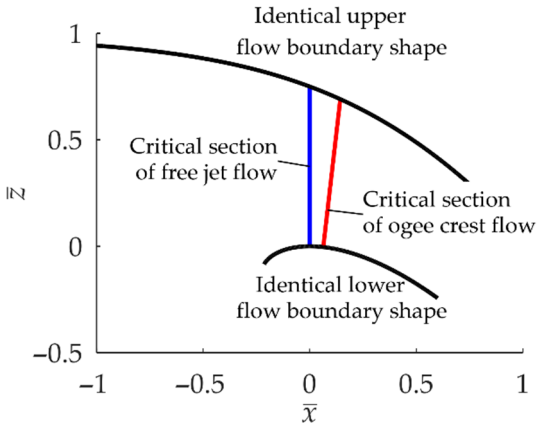

Figure 8. Comparison of a fully ventilated flow over a sharp-crested weir (free jet flow) and the flow over the corresponding ogee crest for the same head (results of a numerical implementation of the equations presented above). The only difference is the position of the critical section.

The fact that the critical section is not at the crest apex makes it unsuitable for the derivation of an analytical model. However, other simplifications are possible at the crest apex.

2.5.2. Approximation at the Crest Apex

The second equation in System (88) makes it clear that for the flow at the design head (which results in $\mathrm{d}\alpha / \mathrm{d}\overline{\xi} = 0$) the following equation is valid everywhere along the crest:

$$\frac{A_\lambda B_\alpha}{A_\alpha B_\lambda} = \frac{B_\alpha S}{A_\alpha T} \tag{91}$$

According to Equations (82), (83), (84), and (87), this corresponds to:

$$\frac{\dfrac{\partial \overline{q}}{\partial \lambda}}{\dfrac{\partial \overline{r}_\mathrm{b}}{\partial \lambda}} = \frac{-\dfrac{\partial \overline{q}}{\partial \theta}\dfrac{\mathrm{d}\theta}{\mathrm{d}\overline{\xi}} - \dfrac{\partial \overline{q}}{\partial \overline{z}_\mathrm{b}}\dfrac{\mathrm{d}\overline{z}_\mathrm{b}}{\mathrm{d}\overline{\xi}}}{\dfrac{\mathrm{d}\overline{r}_\mathrm{b}}{\mathrm{d}\overline{\xi}} - \dfrac{\partial \overline{r}_\mathrm{b}}{\partial \theta}\dfrac{\mathrm{d}\theta}{\mathrm{d}\overline{\xi}} - \dfrac{\partial \overline{r}_\mathrm{b}}{\partial \overline{z}_\mathrm{b}}\dfrac{\mathrm{d}\overline{z}_\mathrm{b}}{\mathrm{d}\overline{\xi}}} \tag{92}$$

i.e., the ratio of the derivatives of $\overline{q}$ and $\overline{r}_\mathrm{b}$ with respect to the velocity coefficient, λ, equals the ratio of the derivatives of the same quantities with respect to the abscissa, $\overline{\xi}$.

When the head ratio, $\overline{H}$, is different from 1, Equation (91) is, strictly speaking, no longer valid everywhere. However, as shown by Equations (89) and (90), Equation (91) is always valid at the critical section. Because of this, it is to be expected that Equation (91) is a good approximation, at least in the vicinity of the critical section. Since the critical section remains close to the crest apex, Equation (91) should also be a good approximation there, i.e., where S equals 0. Given that A_α, B_λ, B_α, and T are never equal to zero, the left-hand side in Equation (91) is zero if $A_\lambda = 0$, which implies:

$$\alpha_0 = \alpha(0) = -\frac{\lambda_0^2(\lambda_0 - 2)}{2\lambda_0 - 1} \tag{93}$$

Moreover, α and λ are also linked through Equation (44). At the crest apex, it reads, with Equation (54):

$$\alpha_0 = \lambda_0^2 - 4\overline{H} \tag{94}$$

Equations (93) and (94) then give the following equation for λ_0:

$$\lambda_0^3 - \lambda_0^2 - \frac{8}{3}\bar{H}\lambda_0 + \frac{4}{3}\bar{H} = 0 \tag{95}$$

This cubic equation can be solved thanks to Cardano's method [38]. Since its discriminant is strictly positive for $\bar{H} > 0$ (for $\bar{H} = 0$, the solution $\lambda_0 = 1$ is obvious), it has three real solutions. The only solution that verifies $\lambda_0 > 1$, in line with (55), is:

$$\lambda_0 = \frac{1}{3} + \frac{2}{3}\left(1 + 8\bar{H}\right)^{1/2} \cos\left\{\frac{1}{3}\cos^{-1}\left[\frac{1 - 6\bar{H}}{\left(1 + 8\bar{H}\right)^{3/2}}\right]\right\} \tag{96}$$

All other flow features at the crest apex (including discharge, water depth, and pressure) can be derived from Equation (96) (see below).

2.5.3. Formulas for the Flow at the Crest Apex of an Ogee Crest

The above developments are based on the velocity and pressure coefficients, λ and α, defined in Figure 6 . This choice proved decisive in finding a valid approximation near the crest apex and an analytical solution to the corresponding set of equations. For practical purposes, another dimensionless quantity is of convenient use:

$$\delta = -\frac{2}{3} + \frac{2}{3}\left(1 + 8\bar{H}\right)^{1/2} \cos\left\{\frac{1}{3}\arccos\left[\frac{1 - 6\bar{H}}{\left(1 + 8\bar{H}\right)^{3/2}}\right]\right\} \tag{97}$$

Note that δ can be interpreted as an image of the head ratio $\bar{H}$: $\delta = 0$ when $\bar{H} = 0$; $\delta = 1$ when $\bar{H} = 1$; and $\delta \to +\infty$ when $\bar{H} \to +\infty$ (Figure 9).

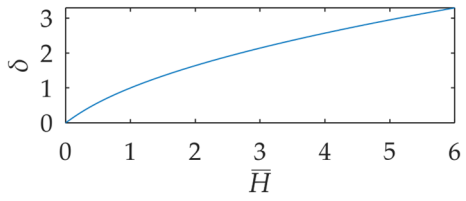

Figure 9. Nonlinear head ratio, δ.

All other flow features at the crest apex can be expressed as rational functions of this nonlinear head ratio, δ.

With Equations (93) and (94), the velocity coefficient at the crest apex reads:

$$\lambda_0 = \delta + 1 \tag{98}$$

With Equations (93) and (98), the pressure coefficient at the crest apex reads:

$$\alpha_0 = \frac{(1 - \delta)(\delta + 1)^2}{2\delta + 1} = \frac{-\delta^3 - \delta^2 + \delta + 1}{2\delta + 1} \tag{99}$$

Given Equations (32), (43), (98), and (99), the discharge coefficient reads:

$$C_d = \frac{q}{\sqrt{2gH^3}} = \frac{2}{3^{3/2}} \frac{\left(\delta^2 + \delta + 1\right)^{1/2}(2\delta + 1)}{(\delta + 1)^2} \tag{100}$$

As shown in Table 2, $C_d = 0.5$ for the design head. For extremely small heads, C_d approaches 0.3849 (but, in this case, the effects of surface tension and viscosity can no longer be neglected). For extremely large heads, C_d approaches 0.7698. This value is also purely theoretical, as nappe separation would occur. However, this value suggests that, even in the absence of nappe separation, C_d cannot be increased endlessly by increasing the head ratio.

With Equations (34), (98), and (99), the ratio of the water depth at the crest apex to the head is:

$$\frac{\overline{h}_0}{\overline{H}} = \frac{h_0}{H} = \frac{(2\delta+1)(\delta+2)}{3(\delta+1)^2} \tag{101}$$

A more common dimensionless bottom pressure than α_0 is, with Equations (99) and (101):

$$\frac{p_{b,0}}{\rho g H} = \alpha_0 \frac{\overline{h}}{\overline{H}} = \frac{(1-\delta)(\delta+2)}{3} \tag{102}$$

Table 2. Values of dimensionless quantities when the head ratio approaches 0, 1, and +∞ (both extremes are hypothetical).

$\overline{H}$	**0**	**1**	**+∞**
δ	0	1	+∞
λ_0	1	2	+∞
α_0	1	0	−∞
C_d	$2/3^{3/2} = 0.3849$	0.5	$4/3^{3/2} = 0.7698$
$p_{b,0}/\rho g H$	2/3	0	−∞
h_0/H	2/3	3/4	2/3

3. Model Validation

The theoretical model presented above gives two types of results: geometrical characteristics of the ideal ogee crest shape and characteristics of the flow over this ideal spillway at the crest apex for a large range of head ratios. These results are presented here and compared to experimental data from several authors. They are also compared to the results of Jaeger's approach (see Section 4 for details).

3.1. Ogee Crest

Since the effect of the slope and curvature of the upper flow boundary on the velocity profile has been neglected or simplified, the theoretical model derived in this paper depends only on the radius of curvature of the crest shape at its highest point—a quantity whose value is a result of the model itself. In this section, the theoretical value $r_b = -H_d/2$ is compared to the radius of curvature of several crest profiles designed for spillways with a vertical upstream face and negligible approach velocities.

Four practical designs are considered in Figure 10 [12]:

1. Type 1: a WES profile with an upstream quadrant composed of three circles of radii 0.04 H_d, 0.2 H_d, and 0.5 H_d and a downstream quadrant given by Equation (105);
2. Type 2: an upstream quadrant described by Equation (103) and a downstream quadrant described by Equation (105);

$$\overline{z}_b = -0.724(\overline{x}_b + 0.270)^{1.85} - 0.126 + 0.4315(\overline{x}_b + 0.270)^{0.625} \tag{103}$$

3. Type 3: an elliptical upstream quadrant given by Equation (104) and a downstream quadrant given by Equation (105);

$$\left(\frac{\overline{x}_b}{0.280}\right)^2 + \left(\frac{\overline{z}_b}{0.167} + 1\right)^2 = 1 \tag{104}$$

4. Type 4: a USBR with an upstream quadrant composed of two circles of radii 0.235 H_d and 0.530 H_d and a downstream quadrant given by Equation (106).

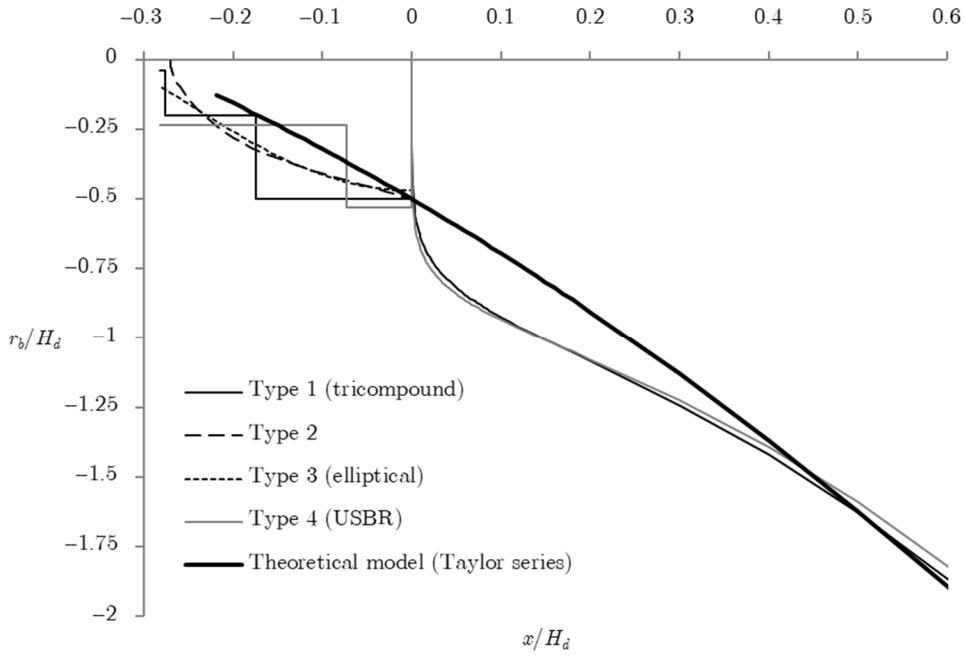

Figure 10. Comparison of the radius of curvature of the theoretical model (Taylor series based on r_b and its two first derivatives at the crest apex, i.e., Equations (54), (57), and (60)) with common crest shapes.

The downstream quadrants (i.e., $x_b > 0$) of all four types are described by a power law. Types 1–3 follow Equation (105), while type 4 follows Equation (106). Note that the radius of curvature at the crest apex is zero for both formulas, which generates a discontinuity with the radius of the upstream quadrant (Figure 10). Nevertheless, the radius of curvature of both formulas increases very rapidly and reaches values in the order of the upstream quadrant values within a distance less than 0.002 H_d, so it seems unlikely that this discontinuity has a real impact on the physical models or prototypes.

$$\overline{z}_b = -0.5\overline{x}_b^{1.85} \tag{105}$$

$$\overline{z}_b = -0.5\overline{x}_b^{1.872} \tag{106}$$

Types 1 and 2 both have $r_b = -0.5\ H_d$ at the crest apex on the upstream quadrant, which is exactly the value of the theoretical model; type 3 has $r_b \approx -0.47\ H_d$ (difference of 6%); and type 4 has $r_b = -0.53\ H_d$ (difference of 6%). Locally, the values given by the theoretical model are very good. However, the spatial distribution of the radius of curvature shows that its absolute values are generally smaller than those of the practical profiles.

3.2. Discharge Coefficient

At the design head and with a negligible approach velocity, USACE indicates $C_d = 0.502$ for type 3 crests [39], while USBR gives $C_d = 0.492$ for type 4 crests [33]. Both values have been converted to fit Definition (1). The value given by the present model ($C_d = 0.5$) differs from these values by 0.002 and 0.008, respectively. Let ε_q be that difference. According to Equation (107), where the subscript "ref" refers to a reference value (an empirical value, as opposed to the theoretical value), a difference of 0.008 means that the difference in discharge is equal to 0.8% of $(2gH^3)^{1/2}$:

$$\varepsilon_q = \left|C_d - C_{d,ref}\right| = \frac{\left|q - q_{ref}\right|}{\sqrt{2gH^3}} \tag{107}$$

At heads other than the design head, the theoretical discharge coefficient is compared to empirical data by several authors in Figure 11. Datasets from experiments designed to be accurate at large head ratios [5,11] are plotted in Figure 11a, while datasets from experiments focusing on smaller head ratios [6,13] are plotted in Figure 11b. The comparison is limited to head ratios smaller than 5 to avoid measurements influenced by flow separation [5]. The theory compares well with experiments at both large and small head ratios, with a tendency to underestimate C_d at head ratios larger than 1.

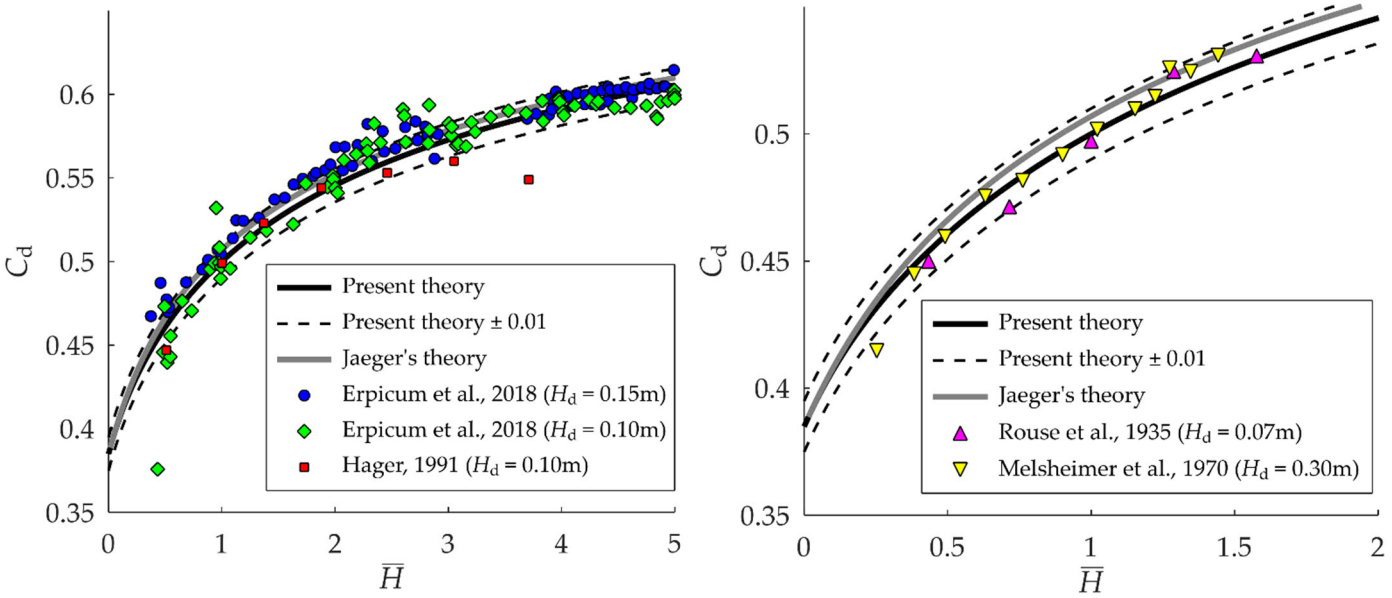

(**a**) (**b**)

Figure 11. Variation in discharge coefficient, C_d, with head ratio: (**a**) for H/H_d = 0 to 5, compared to data from [5,11]; (**b**) for H/H_d = 0 to 2, compared to data from [6,13].

The mean and maximum differences, as defined by Equation (107), are presented in Table 3. Figure 11 shows that the largest differences between theory and experiments occur for head ratios smaller than 1 on experimental setups designed to study large head ratios, that is, for situations in which the measurement errors generate large uncertainties on the value of the discharge coefficient [5]. For example, in the case of the point from [5] (H_d = 0.10 m) with a 7.8% difference between theory and experiments (Table 3)—this point is easily identifiable in Figure 11a—the 7.8% difference is smaller than the uncertainty on the measurement. If this point is taken out of the dataset, the maximum difference is less than 3.6% for all datasets, and the mean difference is less than 0.9%.

Table 3. Comparison of the present theory (and Jaeger's theory) with experimental data. Differences are computed for H/H_d ranging from 0 to 5 (i.e., no flow separation). For Hager's data, the point H/H_d = 3.71 is excluded from the error computation because it seems to be influenced by flow separation.

Reference	Present Theory		Jaeger's Theory	
	Mean ε_q	Maximum ε_q	Mean ε_q	Maximum ε_q
Erpicum et al. [5] (H_d = 0.15 m)	0.8%	3.1% (H/H_d = 0.459)	0.5%	2.6% (H/H_d = 0.459)
Erpicum et al. [5] (H_d = 0.10 m)	0.9%	7.8% (H/H_d = 0.433)	1.0%	8.3% (H/H_d = 0.433)
Hager [11]	0.7%	1.5% (H/H_d = 0.510)	1.1%	2.0% (H/H_d = 0.510)
Rouse et al. [6]	0.4%	1.7% (H/H_d = 0.253)	0.6%	2.0% (H/H_d = 0.253)
Melsheimer et al. [13]	0.5%	0.9% (H/H_d = 0.715)	0.8%	1.5% (H/H_d = 0.715)

3.3. Velocity Distribution

Equations (16) and (25) give the detail of the velocity profiles whose integration give the C_d values above, as shown in Figure 12 in comparison to experimental data from the literature. Note that the experimental data in Figure 12a,b are not available for the whole cross section, only the lower part of it. Moreover, in contrast to [15], the measurements presented in Figure 12a,b were not taken along an isopotential line but along a vertical cross section so that they could be compared to the theoretical model. Finally, note that the velocities in Figure 12a,b are the horizontal velocity component, while the values in Figure 12c are absolute flow velocities.

Within the flow, the results from the model developed in this paper mostly compare well with experimental data but have a tendency to underestimate velocities, which is consistent with the slight underestimation of the discharge coefficient. Close to the interface between the crest and the flow, the effect of the boundary layer can be seen at large head ratios. It leads to a significant decrease in the local velocities compared to the theoretical model.

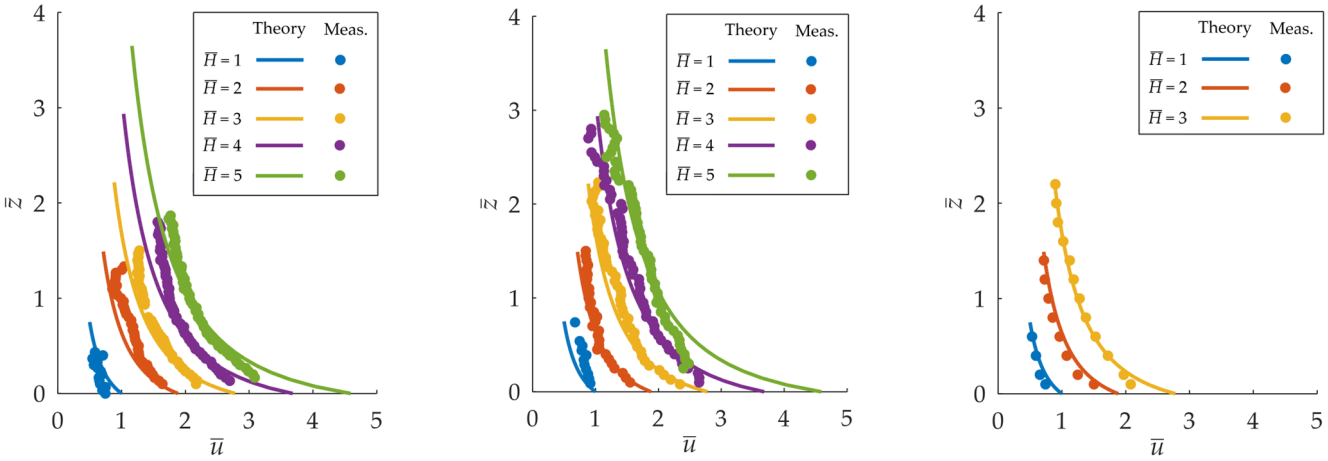

Figure 12. Variation in the velocity distributions with head ratio: comparison with experimental data by (**a**) Peltier et al. [15], H_d = 0.15 m; (**b**) Peltier et al. [15], H_d = 0.10 m; and (**c**) Hager [11]. Dimensionless velocities are defined as $\bar{u} = u / \sqrt{2gH_d^3}$.

3.4. Water Depth at the Crest Apex

The dimensionless water depth given by Equation (101) is compared to experimental data by several authors in Figure 13. Note that there is currently a lack of accurate measurements at large heads, which is why the comparison of the theory and experiments is limited to only two datasets. However, these data are sufficient to confirm the behavior of h/H for increasing head ratios, which reaches a maximum of about 0.75 at the design head.

Let ε_h be the difference between a theoretical value, h/H, and a measured value, h_{ref}/H:

$$\varepsilon_h = \left| \frac{h}{H} - \frac{h_{ref}}{H} \right| = \frac{|h - h_{ref}|}{H} \tag{108}$$

For both datasets, the mean difference is less than 0.5%, and the maximum difference is 1.2% (at H/H_d = 0.153), which means that the difference on h is, on average, less than 0.5% of H. This very good agreement confirms that the slight underestimation of the theoretical discharge coefficient compared to the measurements is due to a slight underestimation of the velocities, rather than a difference in the water depth.

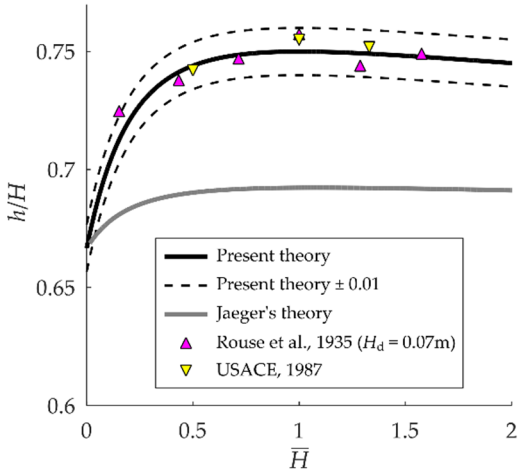

Figure 13. Variation in dimensionless water depth, h/H, at the crest apex with head ratio and comparison with experimental data from [6,39].

3.5. Crest Pressure at the Crest Apex

The dimensionless crest pressure given by Equation (102) is compared to experimental data from several authors in Figure 14. Datasets from experiments designed to be accurate at large head ratios are plotted in Figure 14a, while datasets from experiments focusing on smaller head ratios are plotted in Figure 14b. Note that the dashed lines in Figure 14 correspond to a difference of 0.1, not 0.01 as in Figures 11 and 13.

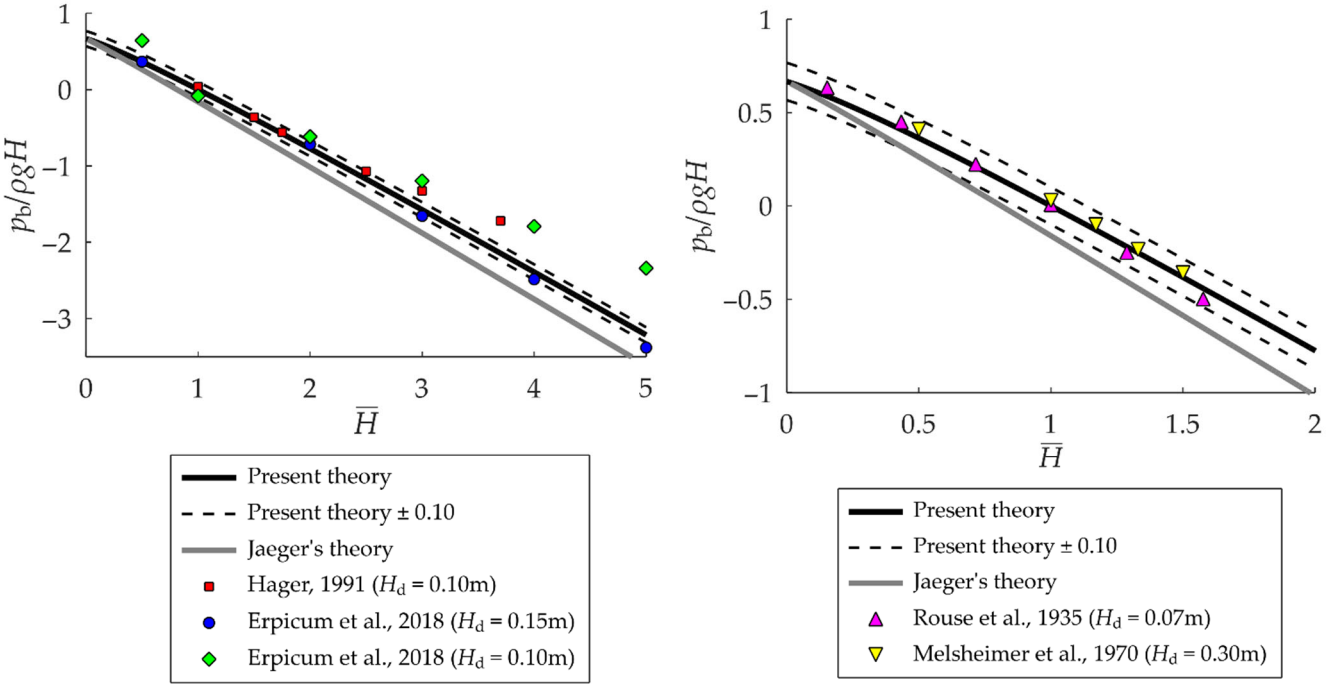

(**a**) (**b**)

Figure 14. Variation in dimensionless crest pressure, $p_b/\rho gH$, at the crest apex with head ratio: (**a**) for H/H_d = 0 to 5, compared with data from [5,11], and (**b**) for H/H_d = 0 to 2, compared with data from [6,13].

Let ε_p be the difference between a theoretical value, $p_b/\rho gH$, and a measured value, $p_{b,ref}/\rho gH$:

$$\varepsilon_p = \left| \frac{p_\mathrm{b}}{\rho g H} - \frac{p_\mathrm{b,ref}}{\rho g H} \right| = \frac{\left| p_\mathrm{b} - p_\mathrm{b,ref} \right|}{\rho g H} \tag{109}$$

At head ratios larger than 2.5, the crest pressures measured on the three scale models plotted in Figure 14a do not agree for an unknown reason. The pressures from the theoretical model generally follow the values of the physical model that generates the lowest pressures, which is the larger model that was tested in [5]. In this case, the mean difference is 8% (that is, the difference in p_b is, on average, equal to 8% of $\rho g H$), with a maximum of 17% at $H/H_\mathrm{d} = 5$. For the datasets of Figure 14b, the mean differences are less than 3.8%, and the maximum differences are less than 5.6%.

3.6. Summary

The above comparison of several outputs of the model developed in this paper with experimental data from the literature shows that the outputs that are influenced most by the approximations of the model are either the radius of curvature of the lower flow boundary or the bottom pressure, depending on the boundary condition (imposed pressure or imposed shape). The values of the discharge coefficient and the relative water depth are less sensitive to these approximations. The theoretical model is found to perform well at both small and large head ratios.

4. Discussion

Section 2 provided a more rigorous mathematical analysis of the critical section than the common assumption that it is located at the highest point of an ogee crest. As shown in Figure 8, with the model used here, the location of the critical section is downstream of the crest apex and varies with the head ratio. This figure also shows that the notion of the critical section is dependent on the lower boundary conditions of the flow (atmospheric pressure or fixed geometry)—a result that becomes less surprising when considering that the upper boundary condition can even lead to the disappearance of the notion of the critical section (closed conduits). Moreover, there is no evidence that, for a given set of boundary conditions, the location of the critical section is independent of the flow model. As a result, the position and properties of the critical section should not be postulated outside of the framework of the model used to describe the flow.

The theoretical model presented here does not derive directly from a critical flow condition, even though it could be seen as a generalization of the critical flow condition of the jet flow ($\partial \overline{q} / \partial \lambda = 0$). Equation (91) is effective because the crest profile follows the lower boundary of a free jet flow, which is not the case for other spillway crests.

As stated in the Introduction, Jaeger's model [7,9,34], which uses the same velocity distribution, was initially derived for quasi-circular weirs, but it was also applied to ogee crests. Jaeger's model assumes $\partial \overline{q} / \partial \overline{h} = 0$ at the crest apex (which is valid for $\mathrm{d}\overline{r}_\mathrm{b} / \mathrm{d}\overline{\xi} = 0$), while the present model assumes $\partial \overline{q} / \partial \lambda = 0$ (which considers $\mathrm{d}\overline{r}_\mathrm{b} / \mathrm{d}\overline{\xi} = 0$ on an ogee crest). The results of Jaeger's model, presented in Section 3, assume $r' = -2$ (cf. [9]) and $\overline{r}_b = -1/2$ (in Jaeger's model, $\overline{r}_b$ is not a result but a parameter). Therefore, the differences between the results of both theories only depend on which partial derivative is considered equal to 0 at the highest point of the spillway.

As shown in Figure 11 and Table 3, Jaeger's theory gives good results for C_d. For one of the experimental datasets ([5]—$H_\mathrm{d} = 0.15$ m) it is even more accurate than the present theory. For the other datasets, the new model is more accurate. The fact that both models give similar results underlines the stability that comes from computing q by equating a derivative of it to 0: changes in the variables cannot have large impacts on the discharge.

The picture is, however, different when it comes to the water depth and the crest pressure (Figures 13 and 14). Jaeger's model accurately predicts C_d due to underestimated

water depths and crest pressures, i.e., overestimated bottom velocities. The present theory predicts these quantities more accurately and, therefore, is more consistent.

5. Conclusions

A theory was developed to compute the discharge coefficient of an ogee crest together with the water depth and crest pressure at the highest point of the profile. The velocity distribution (and its corresponding pressure distribution) used in this theory lead to a one-dimensional curvilinear model for which the notion of a critical section was unambiguous. This velocity distribution also avoided empirical parameters and had only one parameter that needed to be guessed, i.e., the derivative r' of the radius of curvature of the streamlines with respect to the distance normal to the streamlines. This parameter was set equal to –2 because it made a fully analytical treatment of the equations possible, and it was verified that this value is a priori close enough to the actual one to have only a small impact on the discharge.

The new model was first applied to compute the design flow and, consequently, the profile of the crest. It showed that the critical section of the jet flow is located at the highest point of the lower boundary of the flow and gave a radius of curvature of $|r_b| = H_d/2$, consistent with common ogee crest profiles, despite being slightly smaller.

The model was then applied to flows over the ideal ogee profile, as defined in the previous step. This showed that the critical section of this flow is different from the critical section of the design flow (jet flow) because of the difference in the lower boundary condition. It is located downstream of the highest point of the profile and varies with the head ratio. Because of this, the present theory could not be based on a critical flow condition, which would have required numerical methods to find the position of the critical section.

This difficulty was circumvented by considering the balance between two dimensionless quantities: the ratio of the partial derivatives of the specific discharge and the radius of curvature with respect to the velocity coefficient, and the ratio of the partial derivatives of the same quantities with respect to the curvilinear abscissa. Because this balance is perfect along the whole crest profile at design flow and at the critical section for all head ratios, it was assumed that it remains approximately valid for all head ratios at the crest apex because of its proximity with the critical section.

An extensive comparison of the outputs of the theoretical model with several datasets available from different authors showed that the model is consistent and provides very similar results on a range of head ratios between 0 and 5, as long as there is no flow separation. It predicts the discharge with a mean difference below 0.9% of $(2gH^3)^{1/2}$. At the crest apex, it also predicts the water depth, with a mean difference below 0.5% of H (data available for $H/H_d < 2$ only), and the crest pressure, with a mean difference below 8% of ρgH for the data points related to the largest weir tested. The discharge and water depth are therefore well-reproduced by the new model, while the crest pressure and the radius of curvature are more sensitive to the approximations of the present theory.

In this paper, the sets of equations for the jet flow and the flow over a fixed structure were only applied locally and analytically, but they could also be used numerically to compute the whole flow. A better understanding of these equations could be used to design ogee crest profiles that generate less negative crest pressures and decrease cavitation risk and flow detachment risk while keeping almost the same discharge coefficient.

Author Contributions: Conceptualization, F.S., M.P. and S.E.; methodology, M.P., B.D., P.A. and S.E.; developments, F.S. and M.P.; validation, F.S., M.P., Y.P., B.D., P.A. and S.E.; writing—original draft preparation, F.S., M.P. and S.E.; writing—review and editing, F.S., M.P., B.D. and S.E.; supervision, M.P. and S.E. All authors have read and agreed to the published version of the manuscript.

Funding: This research received no external funding.

Data Availability Statement: Not applicable.

Conflicts of Interest: The authors declare no conflict of interest.

References

1. Hager, W.H.; Schleiss, A.J.; Boes, R.M.; Pfister, M. *Hydraulic Engineering of Dams*; CRC Press: London, UK, 2020; ISBN 978-0-203-77143-3.
2. Falvey, H.T. Cavitation. In *Chutes and Spillways*; United States Department of the Interior, Bureau of Reclamation: Denver, CO, USA, 1990.
3. USACE. *Hydraulic Design of Spillways*; U.S. Army Corps of Engineers: Washington, DC, USA, 1990.
4. Abecasis, F.M. Discussion of "Designing Spillway Crests for High-Head Operation". *J. Hydraul. Div.* **1970**, *96*, 2654–2658. https://doi.org/10.1061/JYCEAJ.0002821.
5. Erpicum, S.; Blancher, B.; Vermeulen, J.; Peltier, Y.; Archambeau, P.; Dewals, B.; Pirotton, M. Experimental Study of Ogee Crested Weir Operation Above the Design Head and Influence of the Upstream Quadrant Geometry. In Proceedings of the 7th International Symposium on Hydraulic Structures, Aachen, Germany, 15 May 2018.
6. Rouse, H.; Reid, L. Model Research on Spillway Crests. *Civ. Eng.* **1935**, *5*, 10–14.
7. Castro-Orgaz, O.; Hager, W.H. Non-Hydrostatic Free Surface Flows. In *Advances in Geophysical and Environmental Mechanics and Mathematics*, 1st ed.; Springer: Berlin/Heidelberg, Germany, 2017; ISBN 978-3-319-47971-2.
8. Hager, W.H.; Schleiss, A.J. *Constructions Hydrauliques: Écoulements Stationnaires*; Presses Polytechniques et Universitaires Romandes: Lausanne, Switzerland, 2009; ISBN 978-2-88074-746-6.
9. Jaeger, C. Remarques sur quelques écoulements le long de lits à pente variant graduellement. *Schweiz. Bauztg.* **1939**, *114*, 231–234.
10. Cassidy, J.J. Designing Spillway Crests for High-Head Operation. *J. Hydraul. Div.* **1970**, *96*, 745–753. https://doi.org/10.1061/JYCEAJ.0002376.
11. Hager, W.H. Experiments on Standard Spillway Flow (Including Appendix). *Proc. Inst. Civ. Eng.* **1991**, *91*, 399–416. https://doi.org/10.1680/iicep.1991.15622.
12. Maynord, S.T. *General Spillway Investigation: Hydraulic Model Investigation*; U.S. Army Engineer Waterways Experiment Station: Vicksburg, MS, USA, 1985.
13. Melsheimer, E.S.; Murphy, T.E. *Investigations of Various Shapes of the Upstream Quadrant of the Crest of a High Spillway: Hydraulic Laboratory Investigation*; U.S. Army Engineer Waterways Experiment Station: Vicksburg, MS, USA, 1970.
14. Murphy, T.E. *Spillway Crest Design*; U.S. Army Engineer Waterways Experiment Station: Vicksburg, MS, USA, 1973.
15. Peltier, Y.; Dewals, B.; Archambeau, P.; Pirotton, M.; Erpicum, S. Pressure and Velocity on an Ogee Spillway Crest Operating at High Head Ratio: Experimental Measurements and Validation. *J. Hydro-Environ. Res.* **2018**, *19*, 128–136. https://doi.org/10.1016/j.jher.2017.03.002.
16. Cassidy, J.J. Irrotational Flow Over Spillways of Finite Height. *J. Eng. Mech. Div.* **1965**, *91*, 155–173. https://doi.org/10.1061/JMCEA3.0000692.
17. Ikegawa, M.; Washizu, K. Finite Element Method Applied to Analysis of Flow over a Spillway Crest. *Int. J. Numer. Methods Eng.* **1973**, *6*, 179–189. https://doi.org/10.1002/nme.1620060204.
18. Betts, P.L. A Variational Principle in Terms of Stream Function for Free-Surface Flows and Its Application to the Finite Element Method. *Comput. Fluids* **1979**, *7*, 145–153. https://doi.org/10.1016/0045-7930(79)90030-6.
19. Li, W.; Xie, Q.; Chen, C.J. Finite Analytic Solution of Flow over Spillways. *J. Eng. Mech.* **1989**, *115*, 2635–2648. https://doi.org/10.1061/(ASCE)0733-9399(1989)115:12(2635).
20. Yakun, G.; Xianyun, W.; Chigong, W.; Duo, F. Numerical Modelling of Spillway Flow with Free Drop and Initially Unknown Discharge. *J. Hydraul. Res.* **1998**, *36*, 785–801. https://doi.org/10.1080/00221689809498603.
21. Kim, D.G.; Park, J.H. Analysis of Flow Structure over Ogee-Spillway in Consideration of Scale and Roughness Effects by Using CFD Model. *KSCE J. Civ. Eng.* **2005**, *9*, 161–169. https://doi.org/10.1007/BF02829067.
22. Savage, B.M.; Johnson, M.C. Flow over Ogee Spillway: Physical and Numerical Model Case Study. *J. Hydraul. Eng.* **2001**, *127*, 640–649. https://doi.org/10.1061/(ASCE)0733-9429(2001)127:8(640).
23. Imanian, H.; Mohammadian, A. Numerical Simulation of Flow over Ogee Crested Spillways under High Hydraulic Head Ratio. *Eng. Appl. Comput. Fluid Mech.* **2019**, *13*, 983–1000. https://doi.org/10.1080/19942060.2019.1661014.
24. Dressler, R.F. New Nonlinear Shallow-Flow Equations with Curvature. *J. Hydraul. Res.* **1978**, *16*, 205–222. https://doi.org/10.1080/00221687809499617.
25. Dewals, B.; Erpicum, S.; Archambeau, P.; Detrembleur, S.; Pirotton, M. Depth-Integrated Flow Modelling Taking into Account Bottom Curvature. *J. Hydraul. Res.* **2006**, *44*, 785–795. https://doi.org/10.1080/00221686.2006.9521729.
26. Castro-Orgaz, O. Approximate Modelling of 2D Curvilinear Open Channel Flows. *J. Hydraul. Res.* **2010**, *48*, 213–224. https://doi.org/10.1080/00221681003726353.
27. Ramamurthy, A.S.; Vo, N.-D.; Balachandar, R. A Note on Irrotational Curvilinear Flow Past a Weir. *J. Fluids Eng.* **1994**, *116*, 378–381. https://doi.org/10.1115/1.2910286.
28. Castro-Orgaz, O. Potential Flow Solution for Open-Channel Flows and Weir-Crest Overflow. *J. Irrig. Drain. Eng.* **2013**, *139*, 551–559. https://doi.org/10.1061/(ASCE)IR.1943-4774.0000580.
29. Chow, V.T. *Open-Channel Hydraulics*; McGraw-Hill: New York, NY, USA, 1959.
30. Fischer, G. *Plane Algebraic Curves*; Springer: Berlin/Heidelberg, Germany, 2001; ISBN 978-0-8218-2122-0.
31. Adams, R.A.; Essex, C. *Calculus: A Complete Course*; Pearson Canada: Toronto, ON, Canada, 2010; ISBN 978-0-321-54928-0.
32. Reese, A.J.; Maynord, S.T. Design of Spillway Crests. *J. Hydraul. Eng.* **1987**, *113*, 476–490. https://doi.org/10.1061/(ASCE)0733-9429(1987)113:4(476).

33. USBR. *Design of Small Dams*, 3rd ed.; U.S. Department of the Interior, Bureau of Reclamation: Washington, DC, USA, 1987; ISBN 978-0-16-003373-5.
34. Castro-Orgaz, O. Curvilinear Flow over Round-Crested Weirs. *J. Hydraul. Res.* **2008**, *46*, 543–547. https://doi.org/10.3826/jhr.2008.3251.
35. Hager, W.H. Continuous Crest Profile for Standard Spillway. *J. Hydraul. Eng.* **1987**, *113*, 1453–1457. https://doi.org/10.1061/(ASCE)0733-9429(1987)113:11(1453).
36. Matthew, G.D. On the Influence of Curvature, Surface Tension and Viscosity on Flow over Round-Crested Weirs. *Proc. Inst. Civ. Eng.* **1963**, *25*, 511–524. https://doi.org/10.1680/iicep.1963.10545.
37. Khan, A.A.; Steffler, P.M. Modeling Overfalls Using Vertically Averaged and Moment Equations. *J. Hydraul. Eng.* **1996**, *122*, 397–402.
38. Abramowitz, M.; Stegun, I.A. *Handbook of Mathematical Functions: With Formulas, Graphs and Mathematical Tables*; Dover: New York, NY, USA, 1972; ISBN 978-0-486-61272-0.
39. USACE. *Hydraulic Design Criteria*; U.S. Army Waterways Experiment Station: Vicksburg, MI, USA, 1987.